Transits close to the Lagrangian solutions L_1, L_2 in the Elliptic Restricted Three-body Problem

Rocío I. Paez & Massimiliano Guzzo

Dipartimento di Matematica "Tullio Levi-Civita"

Università degli Studi di Padova

Padova 35122 (PD) Italia

December 1, 2020

Abstract

In the last decades a peculiar family of solutions of the Circular Restricted Three Body Problem has been used to explain the temporary captures of small bodies and spacecrafts by a planet of the Solar System. These solutions, which transit close to the Lagrangian points L_1, L_2 of the CRTBP, have been classified using the values of approximate local integrals and of the Jacobi constant. The use for small bodies of the Solar System requires to consider a hierarchical extension of the model, from the CRTBP to the the full N planetary problem. The Elliptic Restricted Three Body, which is the first natural extension of the CRTBP, represents already a challenge, since global first integrals such as the Jacobi constant are not known for this problem. In this paper we extend the classification of the transits occurring close to the Lagrangian points L_1, L_2 of the ERTBP using a combination of the Floquet theory and Birkhoff normalizations. Provided that certain non-resonance conditions are satisfied, we conjugate the Hamiltonian of the problem to an integrable normal form Hamiltonian with remainder, which is used to define approximate local first integrals and to classify the transits of orbits through a neighbourhood of the Lagrange equilibria according to the values of these integrals. We provide numerical demonstrations for the Earth-Moon ERTBP.

1 Introduction

The mathematics of the close encounters of a small body with a planet has a long story, started with the discoveries of Lexell and Leverrier that planet Jupiter can expel a comet from the Solar System [30]. Today a rich recent literature is concerned with close encounters. See, for example, [12, 17, 5, 6] for analytic studies, [28, 20, 21, 22, 23, 37] for applications to the dynamics of comets, [42, 43, 18, 1] for applications to near-Earth asteroids dynamics and [9, 41, 26, 27, 16, 8, 46, 35] for space mission design. The close encounters occurring with a low relative velocity of the small body with respect to the

Planet are studied, since the paper [9], using a peculiar family of solutions of the Circular Restricted Three Body Problem. These solutions transit close to the Lagrangian points L_1, L_2 of the CRTBP. But, the use for small bodies of the Solar System requires to consider hierarchical extensions of the model, from the CRTBP to the the full N planetary problem, which are still subject of study [2, 24, 25, 40].

The Elliptic Restricted Three Body problem, which represents the first natural extension of the CRTBP, introduces a big change in the dynamics, since no matter how small is the value of the eccentricity, global first integrals such as the Jacobi constant are not known. This problem is defined by the motion of a body P of infinitesimally small mass moving in the gravity field generated by two massive bodies P_1 and P_2 (the primary and secondary body respectively) which move around their common center of mass according to the well known elliptic solutions of the two-body problem. It is usual to represent the motion of P using a rotating-pulsating reference frame (x, y, z) whose origin is in the center of mass of P_1 and P_2, the z axis is orthogonal to the motion of P_1, P_2, and the x, y axes are rotating-pulsating so that the primary and secondary bodies remain at fixed locations on the horizontal axis x. With standard units of measure, the Hamiltonian representing the motions of P in this pulsating-rotating frame is:

$$
\begin{aligned}
h(x, y, z, p_x, p_y, p_z, f; e) = {} & \frac{p_x^2}{2} + \frac{p_y^2}{2} + \frac{p_z^2}{2} - p_y\, x + p_x\, y \\
& + \frac{1}{1 + e\,\cos f} \left(\frac{1}{2}\, e\,(x^2 + y^2 + z^2)\cos f \right. \\
& \left. - \frac{\mu}{\sqrt{(x - (1 - \mu))^2 + y^2 + z^2}} - \frac{1 - \mu}{\sqrt{(x + \mu)^2 + y^2 + z^2}} \right)
\end{aligned}
\tag{1}
$$

where the independent variable, denoted by f, corresponds to the true anomaly of the secondary body, the parameter $\mu \in (0, \frac{1}{2}]$ denotes the reduced mass so that the masses of P_1, P_2 are $1 - \mu, \mu$ respectively, and e denotes the eccentricity of the elliptic motion.

The main advantage of using rotating–pulsating variables is that the Hamilton equations of (1) have five equilibrium points $L_1, \ldots, L_5$ which are located in the same orbital positions $(x_{L_i}, y_{L_i}, 0)$ of the corresponding circular problem characterized by the same value of μ. We here focus our analysis on the collinear equilibrium points L_1, L_2 identified by $(x, y, z, p_x, p_y, p_z) = (x_{L_i}, 0, 0, 0, x_{L_i}, 0)$. For each selected equilibrium L_i it is convenient to introduce variables $(\mathbf{q}, \mathbf{p}) = (q_1, q_2, q_3, p_1, p_2, p_3)$:

$$
\begin{aligned}
x &= q_1 + x_{L_j}, & p_x &= p_1, \\
y &= q_2, & p_y &= p_2 + x_{L_i}, \\
z &= q_3, & p_z &= p_3
\end{aligned}
\tag{2}
$$

such that the equilibrium point L_i is in the origin of the phase-space, and consider the Taylor expansion of h in $(\mathbf{q}, \mathbf{p})$:

$$
H(\mathbf{q}, \mathbf{p}, f; e) = H_2 + H_3 + \ldots
\tag{3}
$$

where each term $H_j(\mathbf{q}, \mathbf{p}, f; e)$ is a polynomial of degree j in the variables $(\mathbf{q}, \mathbf{p})$. Notice that the zero-order term $H_0(f; e)$ has been removed from the Hamiltonian, and the term of order 1 vanishes because we are expanding the Hamiltonian at an equilibrium point.

Since paper [9], the dynamics originating at the Lagrangian points L_1, L_2 of the CRTBP have been used to study the transits of motions at low energies between the regions of the space which are 'internal' or 'external' with respect to the two massive bodies. The analysis is obtained from two properties of the CRTBP: the existence of a global first integral, the so-called Jacobi integral, and of the center, stable and unstable manifolds originating at the equilibria L_1, L_2. In fact, close to a center-center-saddle equilibrium point of a Hamiltonian system, provided that certain non-resonance conditions are satisfied, the Hamiltonian has Birkhoff normal forms of large order:

$$K(\mathbf{Q}, \mathbf{P}) = K_2(\mathbf{Q}, \mathbf{P}) + K_4(\mathbf{Q}, \mathbf{P}) + \ldots + K_N(\mathbf{Q}, \mathbf{P}) + R_{N+1}(\mathbf{Q}, \mathbf{P}) , \qquad (4)$$

where $(\mathbf{Q}, \mathbf{P})$ are canonical variables defined in a neighbourhood of the equilibrium point[1]; each term $K_j(\mathbf{Q}, \mathbf{P})$ is an autonomous polynomial of degree j in the variables $(\mathbf{Q}, \mathbf{P})$ and is integrable, in the sense that it depends on the variables only through the combinations $(Q_1^2 + P_1^2)/2$, $(Q_2^2 + P_2^2)/2$ and $Q_3 P_3$. $R_{N+1}(\mathbf{Q}, \mathbf{P}, f; e)$ is the remainder of the Taylor expansion of K, containing polynomials from order $N + 1$. In [9] only the linear approximation and the planar problem were considered (i.e. $N = 2$ and $Q_3 = P_3 = 0$ in (4)), but later higher non-linear normal forms were computed, as in [41, 26, 15, 36, 16, 33, 27, 13, 29, 23, 38, 37], etc. In these papers the dynamics of transits is obtained by approximating a Birkhoff normal form (4) of large order N with the integrable Hamiltonian (we refer to [39, 34] for an introduction to polynomial normal forms):

$$\mathcal{K}(\mathbf{Q}, \mathbf{P}) = K_2(\mathbf{Q}, \mathbf{P}) + K_4(\mathbf{Q}, \mathbf{P}) + \ldots + K_N(\mathbf{Q}, \mathbf{P}). \qquad (5)$$

From the values of the first integrals of Hamiltonian (5),

$$\mathcal{I}_1 = \frac{Q_1^2 + P_1^2}{2} \ , \mathcal{I}_2 = \frac{Q_2^2 + P_2^2}{2} \ , \ \mathcal{I}_3 = Q_3 P_3 \ ,$$

one obtains a complete classification of the transit orbits according to the approximate Hamiltonian (5). In fact, fixed values of $\mathcal{I}_1, \mathcal{I}_2 \geq 0$ and $Q_3, P_3 = 0$ define an invariant manifold $\mathcal{M}_{\mathcal{I}_1, \mathcal{I}_2}$ for the flow $\phi_{\mathcal{K}}$ of Hamiltonian $\mathcal{K}$ supporting quasi-periodic motions, and the set $Q_3 = 0, P_3 \neq 0$ (resp. $Q_3 \neq 0, P_3 = 0$) defines the local stable (resp. unstable) manifold of $\mathcal{M}_{\mathcal{I}_1, \mathcal{I}_2}$. The values of $\mathcal{I}_3 \neq 0$ identify the transit properties: either the motions approach the Lagrange equilibrium arriving from the direction of P_1 or P_2 and then bounce back, either they transit from one side to the other one of the equilibrium point. The stable and unstable manifolds of $\mathcal{M}_{\mathcal{I}_1, \mathcal{I}_2}$ are separatrices for the transit properties. Moreover, the conservation of the Jacobi integral forces all the low energy transits to occur close the Lagrangian points, due to the peculiar shape of the realms of admissible motions, forming a bottleneck close to L_1, L_2.

This description of the dynamics close to L_1, L_2 is obtained by neglecting the remainder $R_{N+1}(\mathbf{Q}, \mathbf{P})$, and therefore is affected by errors. By considering also the remainder R_{N+1}, the functions $\mathcal{I}_j$ may not be first integrals for the non approximated Hamiltonian K. In particular, while a center manifold survives the perturbation, its invariant tori could not,

---

[1]Note that in the variables $(\mathbf{Q}, \mathbf{P})$ the couple Q_3, P_3 is no more identified with the vertical variables. The planar problem is instead obtained for $Q_2, P_2 = 0$.

and a KAM theory should be implemented. Instead, the errors due to the remainder R_{N+1} are less effective on the transits which occur in short time intervals, we refer to Section 2 for more details.

In this paper we show how the previous discussion about transit orbits extends to the elliptic restricted three–body problem, despite the lack of a global first integral. In the ERTBP the Lagrangian points remain equilibria of the non-autonomous Hamilton equations of (1) and are therefore fixed points of the Poincaré map defined by the Hamiltonian flow at time 2π of the Hamilton equations of (1). Therefore, at least for small values of the eccentricity, one may still follow the road to define center, stable and unstable manifolds of the Poincaré map, providing motions which librate close to the Lagrangian points, as well as motions which are asymptotic to these librations. Unfortunately, these motions would apparently be less useful for the characterization of the transits since global first integrals are not known for the ERTBP. Therefore, on the one hand we cannot define the realms of motions which are forbidden or admissible for a certain value of the Jacobi integral, thus making impossible a sharp definition of transit motion; on the other hand we are not able to identify invariant 3-dimensional (5-dimensional for the spatial problem) level sets of the phase–space disconnected by stable and unstable manifolds related to the dynamics originating at L_1, L_2.

To overcome these issues we construct local normal forms for the Hamiltonian (1), which we call Floquet-Birkhoff normal forms, which are integrable and autonomous up to a suitable large order N:

$$K(\mathbf{Q}, \mathbf{P}, f; e) = K_2(\mathbf{Q}, \mathbf{P}; e) + K_4(\mathbf{Q}, \mathbf{P}; e) + \ldots + K_N(\mathbf{Q}, \mathbf{P}; e) + R_{N+1}(\mathbf{Q}, \mathbf{P}, f; e) \quad (6)$$

where $(\mathbf{Q}, \mathbf{P})$ are canonical variables defined in a neighbourhood $\mathcal{B}$ of the selected Lagrangian point L_i; each term $K_j(\mathbf{Q}, \mathbf{P}; e)$ is an autonomous polynomial of degree j in the variables $(\mathbf{Q}, \mathbf{P})$ and is integrable in the sense that it depends on the $(\mathbf{Q}, \mathbf{P})$ only through the combinations $(Q_1^2 + P_1^2)/2$, $(Q_2^2 + P_2^2)/2$ and $Q_3 P_3$. The Taylor expansion of the remainder $R_{N+1}(\mathbf{Q}, \mathbf{P}, f; e)$ contains polynomials from order $N + 1$, and is possibly dependent periodically on f. The first term of the expansion,

$$K_2(\mathbf{Q}, \mathbf{P}; e) = \sigma_1 \frac{Q_1^2 + P_1^2}{2} + \sigma_2 \frac{Q_2^2 + P_2^2}{2} + \lambda Q_3 P_3 \, ,$$

represents the linear approximation of the system obtained from a Floquet transformation defined at the Lagrange equilibrium and an additional linear transformation which puts to evidence the center-center-saddle nature of the equilibrium. A combination of the Floquet theory and Birkhoff normalizations has been used to study the stability of transversely elliptic periodic orbits [31, 32], and for the equilateral equilibria L_4, L_5 of the ERTBP [44]. The development of the Floquet-Birkhoff normal form (6) at the equilibria L_1, L_2 meets additional complexity in the control of the numerical precision and in the definition of the Floquet transformation. On one hand, the partially hyperbolic nature of these equilibrium points may be responsible of large errors in the computation of the coefficients of the normal form. On the other hand, we need to fix a gauge in the definition of the Floquet transformation. As it is well know, the Floquet transformation is not unique, since its

definition depends on the arbitrary choice of a logarithm of the monodromy matrix $\mathbf{\Phi_e}$, computed at the Lagrange equilibrium. If one is interested only in the dynamics of the Hamilton equations linearized at the equilibrium point, as in the traditional Floquet theory, any choice of the logarithm of $\mathbf{\Phi_e}$ can be used to define the Floquet transformation. But, since our project is to improve the Floquet approximation to higher orders, we need to select the logarithm of the monodromy matrix providing a close to the identity Floquet transformation. In fact, if the Floquet transformation is not close to the identity, the Fourier expansion with respect to f of the transformed Hamiltonian contains a large number of terms with large coefficients, so that the computation of the Birkhoff normal forms saturates the computer memory at low normalization orders N. All the technical details about the Floquet transformation that we use and the Birkhoff transformations providing the normal form (6) will be given in Section 3.

Finally, we describe the transits which occur close to the Lagrangian points using the dynamics of the approximated Hamiltonian:

$$\mathcal{K}(\mathbf{Q}, \mathbf{P}; e) = K_2(\mathbf{Q}, \mathbf{P}; e) + K_4(\mathbf{Q}, \mathbf{P}; e) + \ldots + K_N(\mathbf{Q}, \mathbf{P}; e) \tag{7}$$

which is obtained by neglecting the small remainder $R_{N+1}(\mathbf{Q}, \mathbf{P} f; e)$ in the Floquet-Birkhoff normal form (6).

This paper is organized as follows. Section 2 is dedicated to an overview of the results about the dynamics of the ERTBP that follow from the construction of the Floquet-Birkhoff normal forms (6). In Section 3 we provide all the analytic details of the construction of the Floquet-Birkhoff normal forms. In Section 4 we show the application of the method for the Earth-Moon Elliptic three-body problem. Finally, we provide Conclusions.

2   An overview of the results about the dynamics of the ERTBP following from the Floquet-Birkhoff normal forms

In this Section we present an overview of the key consequences of the existence of Floquet-Birkhoff normal forms on the dynamics of the ERTBP. We denote by $\mathcal{B}$ the neighbourhood of the origin in $\mathbb{R}^6$ where the Floquet-Birkhoff normal form is defined. It is not restrictive to assume that $\mathcal{B}$ has the form $\mathcal{B} = B_1(\rho) \times B_2(\rho) \times B_3(\rho)$ where $B_j(\rho)$ is a two-dimensional Euclidean neighbourhood of $(Q_j, P_j) = (0, 0)$ of radius ρ, and that the canonical transformation:

$$(\mathbf{q}, \mathbf{p}) = \Psi(\mathbf{Q}, \mathbf{P}, f; e)$$

conjugating the Floquet-Birkhoff normal form (6) to Hamiltonian (3) is well defined in for all $(\mathbf{Q}, \mathbf{P}) \in \mathcal{B}$ and all $f \in [0, 2\pi]$.

1. Local energy. Since Hamiltonian $\mathcal{K}$ in Eq. (7) is autonomous it is convenient to describe the motions defined by its Hamiltonian flow $\phi_{\mathcal{K}}$ for fixed values κ of the function
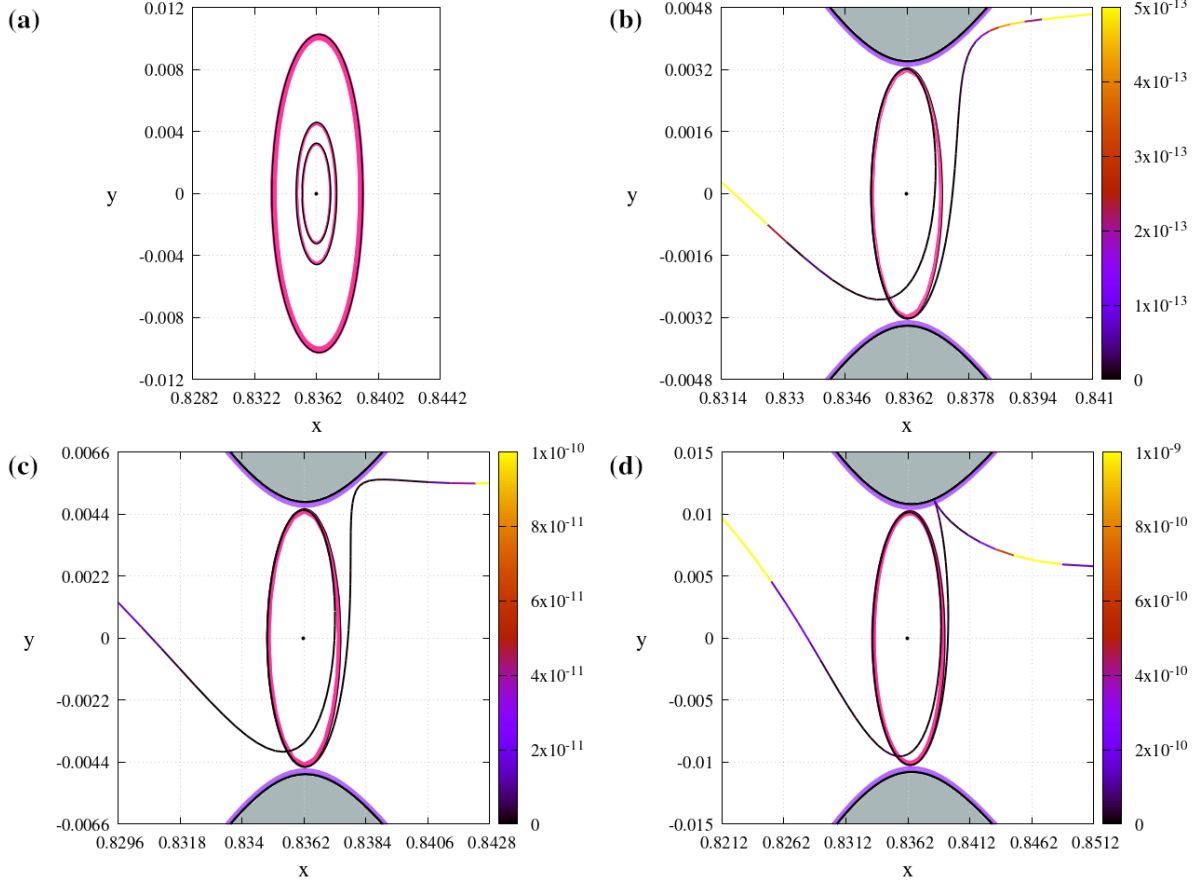
Figure 1: Representation of sample orbits transiting at L_1 for different values of the initial local energy $\kappa = 2.336\times10^{-5}$ (b), 4.672×10^{-5} (c), 2.336×10^{-4} (d), for the planar ERTBP defined by $\mu = 0.0123$, $e = 0.0549006$ (Earth-Moon ERTBP) and normalization order $N = 8$. Panel (a) displays in pink the projection on the Cartesian plane xy of the sets $\mathcal{M}_{\mathcal{I}_{1,0}}$ corresponding to the three values of κ (the section at $f = 0$ for each energy is represented in black); panels (b), (c), (d) display examples of transiting orbits for the aforementioned energies. The initial conditions providing the orbits have been found according to the Floquet-Birkhoff normal forms (more details will be given in Section 4), the orbits have been then obtained by numerically integrating the Hamilton equations of Hamiltonian (1). The orbits are represented using a color scale which indicates the variation of the local energy with respect to the initial value, as the orbit proceeds. The 'zero velocities curves' for all f are in the thin purple bands, delimited on the external side by the black curves; the vector $-\nabla\mathcal{V}_*$ points outward with respect to the shaded gray areas.
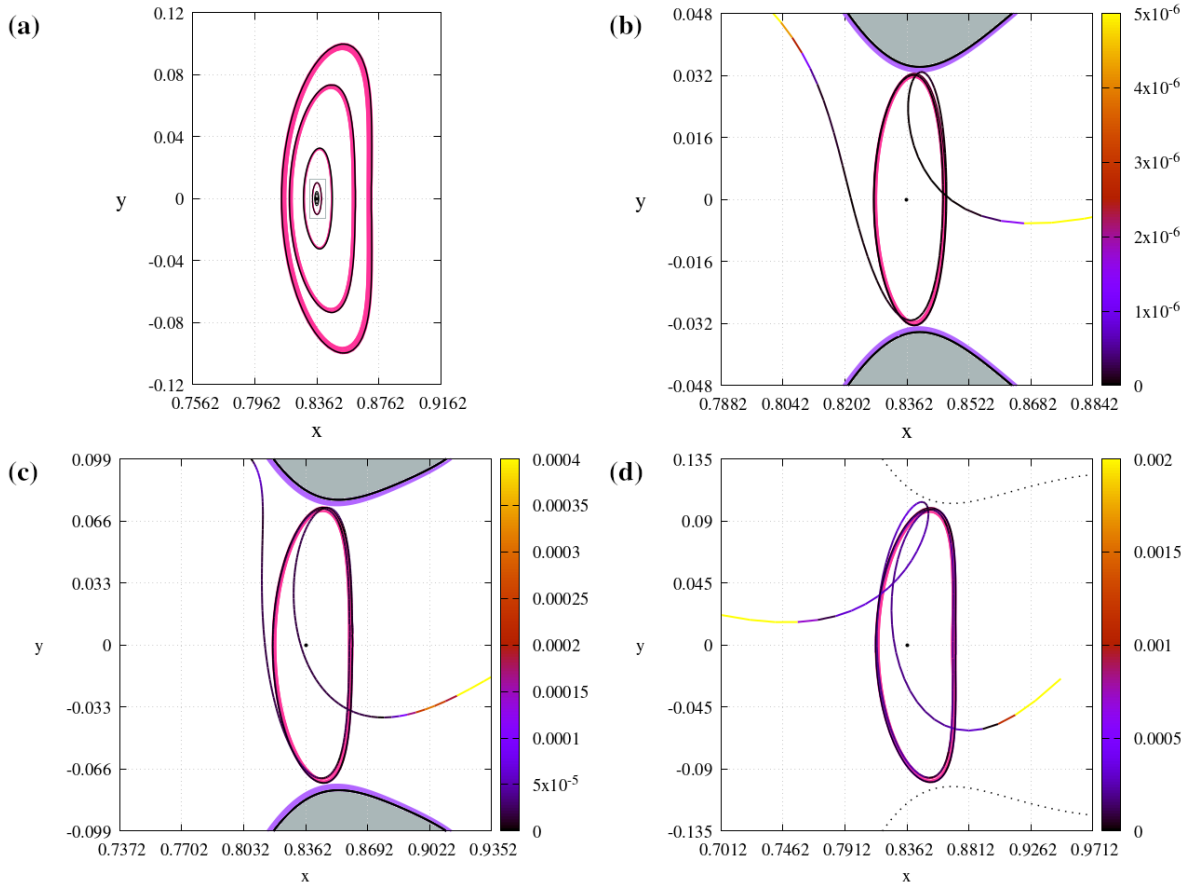
Figure 2: As for Fig. 1 for the larger values of the local energies $\kappa = 2.329 \times 10^{-3}$ (b); $\kappa = 1.150 \times 10^{-2}$ (c) and $\kappa = 2.044 \times 10^{-2}$ (d). To appreciate the larger amplitude of these orbits, we plot a small gray rectangle in panel (a) corresponding to panel (a) of Fig. 1. We do not report the zero velocity curves in panel (d), since for these large libration we expect a good conservation of the local energy only very close to the set $\mathcal{M}_{\mathcal{I}_1,0}$ (see Section 4.2 for more details).

7

$\mathcal{K}$, which we call local energy. In Figures 1 and 2 we provide some examples of conservation of the local energy for solutions of the Earth–Moon ERTBP transiting in a neighbourhood of the Lagrangian point L_1. Since the Lie derivative of the local energy is proportional to the derivatives of the remainder R_{N+1}, the variations of $\mathcal{K}$ in the flow of the complete Hamiltonian are very small closer to the Lagrangian point, as in Figure 1, and become more important for the large librations we reach in the examples of Figure 2.

2. Zero velocity surfaces. By representing the Hamiltonian (7) in the translated Cartesian variables $(\mathbf{q}, \mathbf{p})$ we obtain a function $\hat{\mathcal{K}}(\mathbf{q}, \mathbf{p}; f)$ which is an approximate local first integral defined in a neighbourhood of the Lagrangian point L_i. For any value of f, and any small value κ of the local energy, we define the *zero velocity surfaces* through the equation:

$$\hat{\mathcal{K}}(q_1, q_2, q_3, -q_2, q_1, 0, f; e) = \kappa, \tag{8}$$

and the *zero velocity curves* for the planar problem. In the ERTBP the zero velocity surfaces do not strictly provide a barrier for the motions as for the surfaces obtained from the Jacobi constant for the CRTBP. Nevertheless, since when $\dot{\mathbf{q}} = (0, 0, 0)$ we have $\ddot{\mathbf{q}} = -\nabla \mathcal{V}_*(\mathbf{q}, f; e)$ with

$$\mathcal{V}_*(\mathbf{q}, f; e) = \left(-\frac{1}{2}(x^2 + y^2) + \frac{1}{1 + e \cos f} \left(\frac{1}{2} e (x^2 + y^2 + z^2) \cos f \right. \right.$$
$$\left. \left. - \frac{\mu}{\sqrt{(x - (1 - \mu))^2 + y^2 + z^2}} - \frac{1 - \mu}{\sqrt{(x + \mu)^2 + y^2 + z^2}} \right) \right)_{x = q_1 + x_{L_1}, y = q_2, z = q_3}, \tag{9}$$

the direction of the vector $-\nabla \mathcal{V}_*(\mathbf{q}, f; e)$ at the zero velocity surfaces provide an indication of the repelling effect of the surfaces on the motions (the position of $\mathbf{q}(f)$ should be compared with the surface defined by the value f of the true anomaly). A numerical computation of the zero-velocity curves is reported in Figures 1, 2, where for all the cases the vector $-\nabla \mathcal{V}_*$ points outward with respect to the shaded area.

3. Transit orbits. For $\kappa > 0$ the level set:

$$\mathcal{M}_\kappa = \{(\mathbf{Q}, \mathbf{P}) \in \mathcal{B} : \ \mathcal{K}(\mathbf{Q}, \mathbf{P}; e) = \kappa \ , \ Q_3, P_3 = 0\}$$

contains a collection of sets $\mathcal{M}_{\mathcal{I}_1, \mathcal{I}_2}$ invariant for the approximated flow $\phi_\mathcal{K}$. Its local stable and unstable manifolds $W_\kappa^{s,loc}, W_\kappa^{u,loc}$ are defined by $Q_3 = 0, P_3 \neq 0$ or $Q_3 \neq 0, P_3 = 0$ respectively. The local stable and unstable manifolds are separatrices for the transits occurring close to the Lagrangian point, and we recover from the circular case the classification of transit motions according to the position of the orbits expressed in the variables Q, P with respect to $W_\kappa^{s,loc}, W_\kappa^{u,loc}$.

A transit is defined as a motion $(\mathbf{Q}(f), \mathbf{P}(f))$ of $\phi_\mathcal{K}$ in the interval of $f \in [f_0, f_1]$ such that: $(\mathbf{Q}(f), \mathbf{P}(f)) \in \mathcal{B}$ for all $f \in (f_0, f_1)$, and both endpoints $(\mathbf{Q}(f_0), \mathbf{P}(f_0)), (\mathbf{Q}(f_1), \mathbf{P}(f_1))$ belong to the border of $\mathcal{B}$. Moreover, we have $\mathcal{I}_3 > 0$ along the motion. In fact, since in the approximated flow $\phi_\mathcal{K}$ the variables Q_1, P_1, Q_2, P_2 oscillate periodically, the motion $(\mathbf{q}(f), \mathbf{p}(f))$ is the superposition of quasi-periodic oscillations and of an hyperbolic motion which defines the transit property. For small values of the eccentricity e, the Cartesian

8

variables q_1, q_2 are related to the variables $(\mathbf{Q}, \mathbf{P})$ by

$$
\begin{aligned}
q_1 &= a(Q_3 - P_3) + bP_1 + \dots.. \\
q_2 &= c(Q_3 + P_3) + dQ_1 + \dots..
\end{aligned}
\tag{10}
$$

where a, b, c, d are numbers depending on μ, and the 'dots' indicate both linear contributions which are not present when $e = 0$, or non-linear contributions. Therefore the transits from/to negative to/from positive values of q_1 occur for $\mathcal{I}_3 = Q_3 P_3 > 0$.

In Fig. 3 we represent four transit and non-transit planar orbits whose initial conditions have been chosen using the Floquet-Birkhoff normal form, as well as their projections on the planes of the normalized variables (Q_1, P_1) and (Q_3, P_3). The red and green orbits are of transit type, while the blue and orange orbits are non-transit type. In Figure 4 we represent a family of transit and non–transit orbits obtained from the same initial conditions for the variables $\mathbf{Q}, \mathbf{P}$ used for Fig. 3, but different initial values of f, thus showing the effect of the non null eccentricity. Transit orbits in the spatial case are presented in Section 4.2.

4. Error estimates, local diffusion, Arnold diffusion.
By neglecting the small remainder $R_{N+1}(\mathbf{Q}, \mathbf{P}, f; e)$ we are introducing errors which are mainly due to the fact that the functions $\mathcal{I}_j$ may not be first integrals. Nevertheless, in a neighbourhood of radius ϱ of the equilibrium, their Lie derivatives are small,

$$
\frac{d}{df}\mathcal{I}_j = \{\mathcal{I}_j, R_{N+1}\} = \mathcal{O}(\varrho^{N+1}) \quad j = 1, 2, 3 \ ,
$$

and therefore their cumulative variation

$$
|\mathcal{I}_j(f_1) - \mathcal{I}_j(f_0)| \le |f_1 - f_0| \sup_{(Q,P)\in\mathcal{B}, f\in[f_0,f_1]} |\{\mathcal{I}_j, R_{N+1}\}|
\tag{11}
$$

is small when the transits occur in a small interval $[f_0, f_1]$. The order of normalization N fixes a lower bound on $\mathcal{I}_3 > 0$, such that the transits occurring with larger values of $\mathcal{I}_3$ are well approximated by the transits obtained from the integrable Hamiltonian $\mathcal{K}$.

In fact, let us consider the following argument, which is here presented in an heuristic way. By assuming for simplicity $\mathcal{K} = K_2$, an orbit with $\mathcal{I}_3 > 0$ entering to the set $\mathcal{B}$ at f_0 will exit from $\mathcal{B}$ after a time interval Δf of order:

$$
\Delta f \sim \frac{1}{\lambda} \ln \frac{\rho^2}{\mathcal{I}_3}.
$$

For each given normalization order N there exists a constant C (uniform with respect to the choice of the initial conditions) such that in the same interval the flow of the ERTBP will change the value of $\mathcal{I}_3$ no more than

$$
\Delta \mathcal{I}_3 \le C \Delta f \rho^{N+1} \sim \frac{C}{\lambda} \rho^{N+1} \ln \frac{\rho^2}{\mathcal{I}_3}.
$$

Therefore, for any chosen small ϵ, during the transit the variation of $\mathcal{I}_3$ is smaller than $\epsilon \mathcal{I}_3(f_0)$ as soon as

$$
\frac{\mathcal{I}_3(f_0)}{\ln \frac{\rho^2}{\mathcal{I}_3(f_0)}} \ge \frac{C}{\epsilon\lambda} \rho^{N+1},
$$
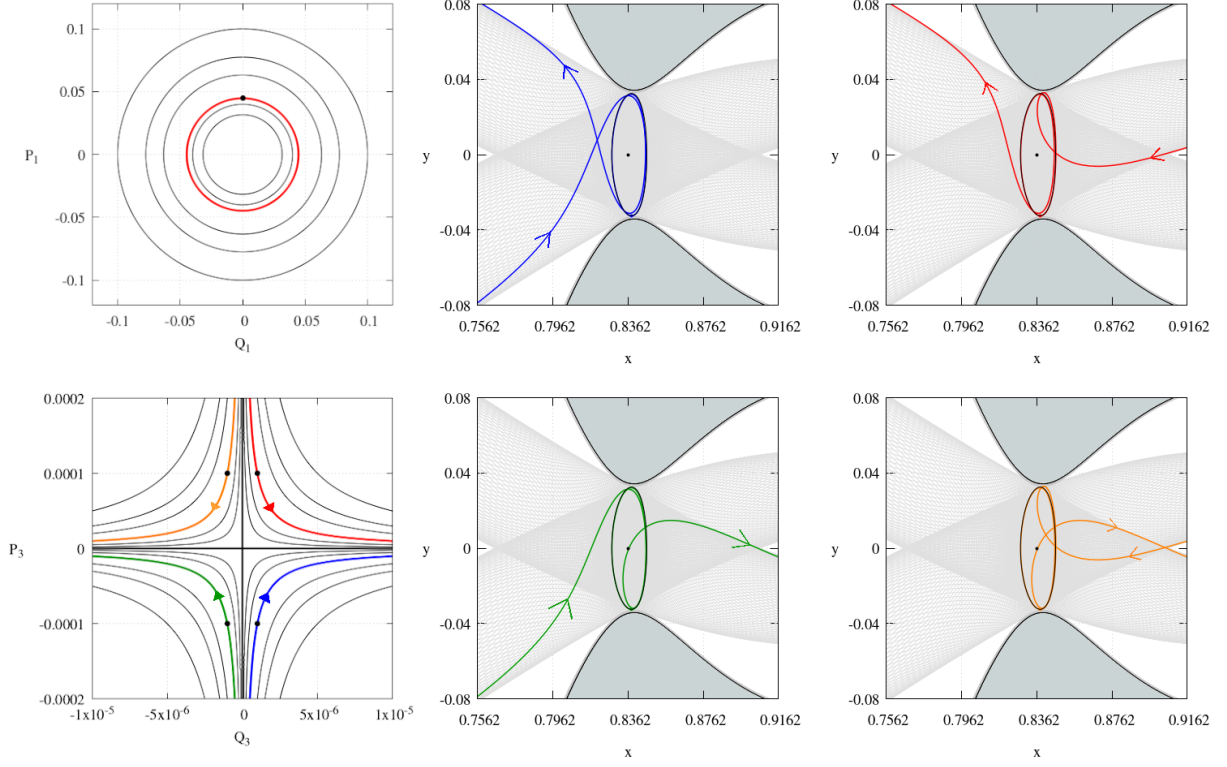
Figure 3: Transit and non-transit orbits numerically computed from initial conditions chosen according to different values of the normalized variables Q_3, P_3. The initial conditions are: $Q_1 = 0$, $P_1 = 1/(10\sqrt{5})$, $Q_2, P_2 = 0$ and $f = 0$ for all the orbits, while $Q_3 = 1\times10^{-6}$, $P_3 = -1\times10^{-4}$ for the blue orbit, $Q_3 = 1\times10^{-6}$, $P_3 = 1\times10^{-4}$ for the red orbit, $Q_3 = -1\times10^{-6}$, $P_3 = -1\times10^{-4}$ for the green orbit and $Q_3 = -1\times10^{-6}$, $P_3 = 1\times10^{-4}$ for the orange orbit. The center and right panels show the projection of the orbits in the original xy Cartesian variables. The left (upper and lower) panels show the projection of the orbits in normalized variable planes (Q_1, P_1) (where the four orbits overlap) and (Q_3, P_3) respectively. The black points are the initial conditions of the orbits. The black elongated curve corresponds to the section $f = 0$ of the 2-d torus $\mathcal{M}_{\mathcal{I}_1,0}$; the gray orbits are in the stable and unstable manifolds of $\mathcal{M}_{\mathcal{I}_1,0}$. The black-bold curves are the zero velocity curves for $f = 0$. The arrows indicate the direction of the motion for increasing values of f.
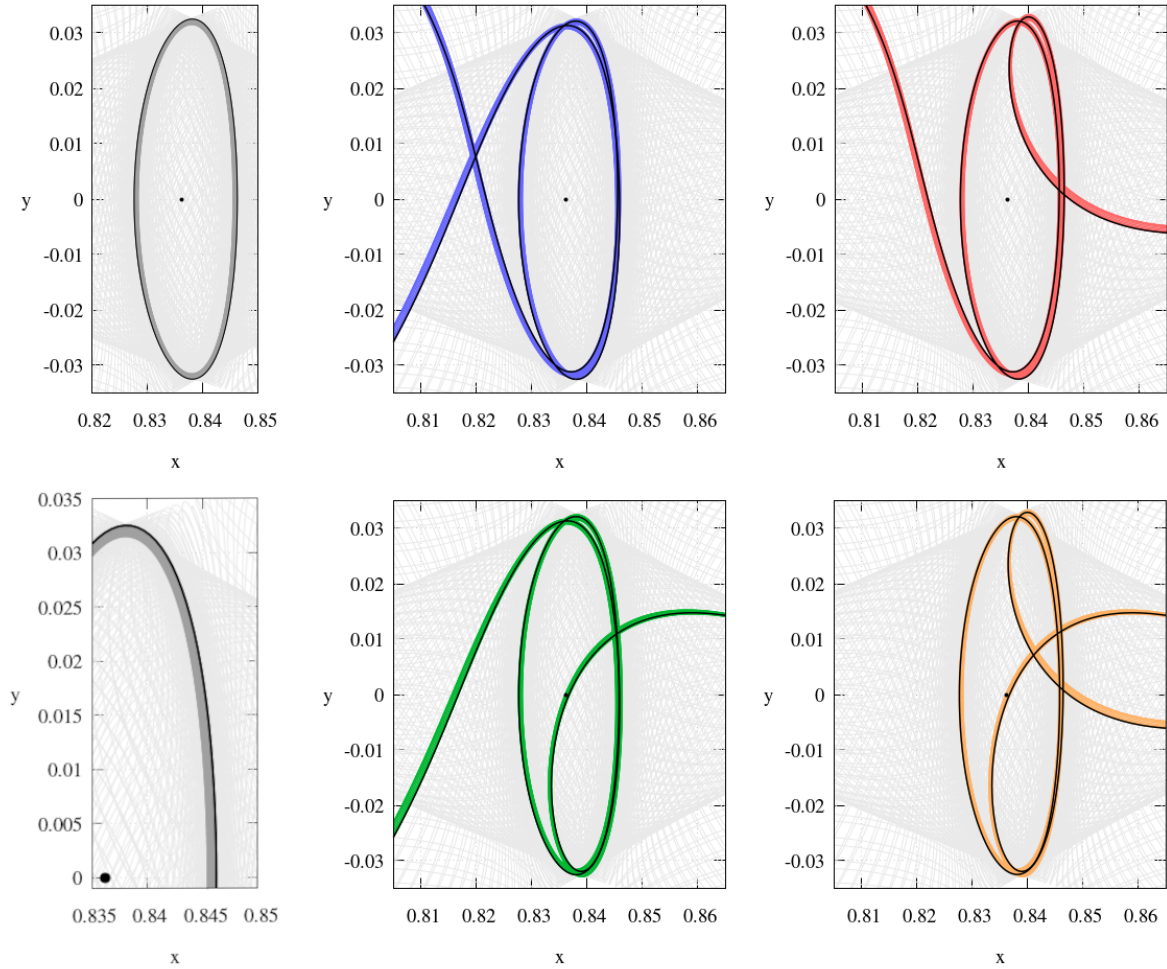
Figure 4: As Figure 3, but considering a set of 15 different initial values of f, instead of a single one, represented as a color band. The amplitude of the bands indicates the influence of the non null eccentricity. In all panels, the black orbit corresponds to the orbits show in the examples of Fig. 3.

11

providing a lower threshold for the value of $\mathcal{I}_3$, depending on the normalization order N. In the time interval Δf the actions $\mathcal{I}_1, \mathcal{I}_2$ (as well as the local energy κ) have small variations according to inequality (11).

Instead, for motions which remain close to $Q_3, P_3 = 0$ for long times, our methods do not allow to rule out the accumulation of errors providing a possible very slow local diffusion of $\mathcal{I}_1, \mathcal{I}_2$, driving the motion outside the set $\mathcal{B}$.

Finally, while each individual transit occurring with values of $\mathcal{I}_3$ satisfying (2) preserves (approximately) the value of the local energy κ up to a very small variation, orbits of the ERTBP which exit the set $\mathcal{B}$ are allowed to re-enter the set $\mathcal{B}$ at a later time with a different value of κ. A similar phenomenon, even if not related to transits but to the homoclinic returns to the center manifold, has been proved for the ERTBP using techniques of Arnold diffusion [4].

3   Floquet-Birkhoff normalization of the Hamiltonian

Let us consider the variables $(\mathbf{q}, \mathbf{p}) = (q_1, q_2, q_3, p_1, p_2, p_3)$ introduced in Eq. (2) and consider the Taylor expansion of h in $(\mathbf{q}, \mathbf{p})$:

$$H(\mathbf{q}, \mathbf{p}, f; e) = H_2 + H_3 + \dots \; , \tag{12}$$

where each term $H_j(\mathbf{q}, \mathbf{p}, f; e)$ is a polynomial of degree j in the variables $(\mathbf{q}, \mathbf{p})$ (notice that the zero-order term $H_0(f; e)$ has been removed from the Hamiltonian and that the term of first order vanishes because we are expanding the Hamiltonian at an equilibrium point). The term of second order is

$$H_2(\mathbf{q}, \mathbf{p}, f; e) = \frac{p_1^2}{2} + \frac{p_2^2}{2} + \frac{p_3^2}{2} - p_2\, q_1 + p_1\, q_2 + \frac{\beta\left(-2q_1^2 + q_2^2 + q_3^2\right)}{1 + e \cos f} + \frac{e \cos f\left(q_1^2 + q_2^2 + q_3^2\right)}{2\left(1 + e \cos f\right)} \tag{13}$$

with

$$\beta = \frac{1}{2}\left(\frac{\mu}{|1 - x_{L_i} - \mu|^3} + \frac{1 - \mu}{|x_{L_i} + \mu|^3}\right) \; . \tag{14}$$

We here use a combination of the Floquet theory and Birkhoff normalizations to conjugate the Hamiltonian (12) to a normal form which is integrable and autonomous up to a suitable large order N:

$$K(\mathbf{Q}, \mathbf{P}, f; e) = K_2(\mathbf{Q}, \mathbf{P}; e) + K_4(\mathbf{Q}, \mathbf{P}; e) + \dots + K_N(\mathbf{Q}, \mathbf{P}; e) + R_{N+1}(\mathbf{Q}, \mathbf{P}, f; e) \; . \tag{15}$$

Each term $K_j(\mathbf{Q}, \mathbf{P}; e)$ is an autonomous polynomial of degree j in the variables $(\mathbf{Q}, \mathbf{P})$ and is integrable, in the sense that it depends on the variables only through the combinations $(Q_1^2 + P_1^2)/2$, $(Q_2^2 + P_2^2)/2$ and $Q_3 P_3$. The remainder $R_{N+1}(\mathbf{Q}, \mathbf{P}, f; e)$ of the Taylor expansion of K contains monomials from order $N + 1$ and is possibly dependent on f. The Floquet-Birkhoff normal form is obtained from the composition of:

(i) a canonical Floquet transformation:

$$(\mathbf{q}, \mathbf{p}) = \mathcal{C}(f; e)(\tilde{\mathbf{q}}, \tilde{\mathbf{p}})$$

12

conjugating the Hamiltonian (12) to an Hamiltonian:

$$\tilde{H}(\tilde{\mathbf{q}}, \tilde{\mathbf{p}}, f; e) = \tilde{H}_2(\tilde{\mathbf{q}}, \tilde{\mathbf{p}}; e) + \tilde{H}_3(\tilde{\mathbf{q}}, \tilde{\mathbf{p}}, f; e) + \dots \qquad (16)$$

where each term $\tilde{H}_j(\tilde{\mathbf{q}}, \tilde{\mathbf{p}}, f; e)$ is polynomial of degree j in the variables $\tilde{\mathbf{q}}, \tilde{\mathbf{p}}$ and periodic in f with period 2π, while $\tilde{H}_2(\tilde{\mathbf{q}}, \tilde{\mathbf{p}}; e)$ is autonomous.

(ii) a linear canonical transformation:

$$(\tilde{\mathbf{q}}, \tilde{\mathbf{p}}) = \mathcal{D}(\hat{\mathbf{Q}}, \hat{\mathbf{P}}) \qquad (17)$$

giving $\tilde{H}_2(\tilde{\mathbf{q}}, \tilde{\mathbf{p}}; e)$ the normal form:

$$k_2(\hat{\mathbf{Q}}, \hat{\mathbf{P}}) = \sigma_1 \frac{\hat{Q}_1^2 + \hat{P}_1^2}{2} + \sigma_2 \frac{\hat{Q}_2^2 + \hat{P}_2^2}{2} + \lambda \hat{Q}_3 \hat{P}_3. \qquad (18)$$

We denote by $k_j(\hat{\mathbf{Q}}, \hat{\mathbf{P}}, f; e)$ the image of all the other polynomials $k_j(\hat{\mathbf{Q}}, \hat{\mathbf{P}}; , f; e) = \tilde{H}_j(\mathcal{D}(\hat{\mathbf{Q}}, \hat{\mathbf{P}}), f; e)$.

(iii) a sequence of $N-2$ Birkhoff transformations giving the Hamiltonian the final normal form (15), which we call Floquet-Birkhoff normal form of order N.

Particular attention must be devoted to the construction of the canonical Floquet transformation (i), whose definition is not unique since it relies on the choice of a logarithm of the monodromy matrix $\boldsymbol{\Phi}_{\mathbf{e}}$ of the Hamiltonian flow of H_2. If one is interested in the dynamics of the linearized Hamiltonian H_2, any choice of the logarithm of $\boldsymbol{\Phi}_{\mathbf{e}}$ can be used to define the Floquet transformation. But, since our project is to make autonomous also polynomials of higher order, we need to select the logarithm of the monodromy matrix providing a close to the identity Floquet transformation

$$\mathcal{C}(f; e) = \mathbb{I} + eC(f; e) \ ;$$

more details will be given in the Subsections below.

The linear transformation (ii) exists provided the monodromy matrix $\boldsymbol{\Phi}_{\mathbf{e}}$ has a couple of real eigenvalues $e^{2\pi\lambda}, e^{-2\pi\lambda} \neq 1$ and two couples of complex conjugate eigenvalues $a_1 \pm ib_1, a_2 \pm ib_2$ with $a_1^2 + b_1^2 = a_2^2 + b_2^2 = 1$, as it happens for $e = 0$.

Finally, the Birkhoff transformations (iii) exist provided the frequencies σ_1, σ_2 appearing in (18) and the frequency $\sigma_3 = 1$ associated to the motion of the primaries have no resonances of order smaller or equal than N:

$$j_1\sigma_1 + j_2\sigma_2 + j_3 \neq 0 \quad \forall(j_1, j_2) \in \mathbb{Z}^2 : \ |j_1| + |j_2| \in [1, N], \quad \forall j_3 \in \mathbb{Z} \ . \qquad (19)$$

Our results improve the Floquet theory for those values of μ, e such that the frequencies σ_1, σ_2 have no resonances of order smaller or equal than $N = 3$. To give an idea of the possible resonances occurring for the lowest values of N, in Table 1 we provide the computation of the resonances for $e = 0$.

	j_1	j_2	j_3	μ
L_1	-1	2	-2	$2.70101{\times}10^{-4}$
L_2	-1	0	-2	$4.00200{\times}10^{-4}$
L_2	-2	0	3	$2.59916{\times}10^{-1}$
L_2	-2	1	2	$3.88166{\times}10^{-3}$
L_2	-1	-1	3	$2.12951{\times}10^{-1}$
L_2	0	2	-3	$1.70749{\times}10^{-1}$

Table 1: Values of μ for which lower order resonances ($N = 3$) occur in the vicinity of L_1 or L_2, see Eq. (19).

3.1 The canonical Floquet Transformation

The Floquet theorem [11] provides a representation of the solutions of periodic linear differential equations of the form

$$\dot{\mathbf{x}} = A(t)\,\mathbf{x} \tag{20}$$

where $\mathbf{x} \in \mathbb{R}^n$ and the matrix $A(t)$ is a regular function of period T. The principal fundamental matrix for the system (20) is the function $\Phi(t)$ whose columns are n linearly independent solutions of (20) such that $\Phi(0) = \mathbb{I}$. The matrix $\mathbf{\Phi} := \Phi(T)$ is usually known as the monodromy matrix and its eigenvalues are the characteristic multipliers of the system. The theorem states that $\Phi(t)$ can be written as

$$\Phi(t) = \mathcal{C}(t)\,\mathrm{e}^{Bt} \qquad \forall\, t \in \mathbb{R} \tag{21}$$

where $\mathcal{C}$ is a non-singular $2T$-periodic function with $\mathcal{C}(0) = \mathbb{I}$ and B is a real matrix satisfying

$$\mathrm{e}^{2TB} = \mathbf{\Phi}^2 \;. \tag{22}$$

When the matrix $A(t)$ is Hamiltonian, the matrix $\mathcal{C}(t)$ can be defined symplectic (see [45]). A key consequence of the theorem is the existence of a time-dependent change of coordinates:

$$\mathbf{x} = \mathcal{C}(t)\,\mathbf{y} \;, \tag{23}$$

conjugating the linear system (20) to the autonomous one:

$$\dot{\mathbf{y}} = B\,\mathbf{y} \;, \tag{24}$$

with B satisfying (22). For our purposes we need to define a canonical Floquet transformation which conjugates H_2 to an autonomous quadratic Hamiltonian. For a different application of the Floquet theory, regarding the stability/instability transition of the normal modes in the circular problem, see [7].

We denote by $\mathbf{x} = (\mathbf{q}, \mathbf{p})$, $\mathbf{y} = (\tilde{\mathbf{q}}, \tilde{\mathbf{p}})$ the phase–space vectors in $\mathbb{R}^6$, and define the

14

matrix $A(f;e)$ by

$$A(f;e) = \mathbb{E}\nabla H_2 = \begin{pmatrix} 0 & 1 & 0 & 1 & 0 & 0 \\ -1 & 0 & 0 & 0 & 1 & 0 \\ 0 & 0 & 0 & 0 & 0 & 1 \\ \frac{4\beta - e\cos f}{1 + e\cos f} & 0 & 0 & 0 & 1 & 0 \\ 0 & -\frac{2\beta + e\cos f}{1 + e\cos f} & 0 & -1 & 0 & 0 \\ 0 & 0 & -\frac{2\beta + e\cos f}{1 + e\cos f} & 0 & 0 & 0 \end{pmatrix}, \qquad (25)$$

where $\mathbb{E}$ is the standard symplectic matrix of $\mathbb{R}^6$. We denote by $\Phi(f;e)$ the principal fundamental matrix solution for the Hamilton equations of H_2, and by $\boldsymbol{\Phi}_e := \Phi(2\pi;e)$ the monodromy matrix. We have the following algebraic lemma.

Lemma. *Assume that the matrix $\boldsymbol{\Phi}_e$ has a couple of real eigenvalues $e^{2\pi\lambda} > e^{-2\pi\lambda}$ and two different couples of complex conjugate eigenvalues $a_1 \pm ib_1$, $a_2 \pm ib_2$ with $a_1^2 + b_1^2 = a_2^2 + b_2^2 = 1$ and $b_1, b_2 > 0$. Then there exists a real symplectic matrix C, which is explicit function of the eigenvectors of $\boldsymbol{\Phi_e}$, such that the matrix defined by*

$$\hat{B}_e(k_1,k_2) = C \begin{pmatrix} 0 & 0 & 0 & \pm(\omega_1 + k_1) & 0 & 0 \\ 0 & 0 & 0 & 0 & \pm(\omega_2 + k_2) & 0 \\ 0 & 0 & \pm\lambda & 0 & 0 & 0 \\ \mp(\omega_1 + k_1) & 0 & 0 & 0 & 0 & 0 \\ 0 & \mp(\omega_2 + k_2) & 0 & 0 & 0 & 0 \\ 0 & 0 & 0 & 0 & 0 & \mp\lambda \end{pmatrix} C^{-1},$$

$$(26)$$

where

$$\omega_j = \frac{1}{2\pi}\arccos(a_j) \quad, \quad j = 1,2 \qquad (27)$$

k_1, k_2 *are arbitrary integer numbers and the choice of the signs in the matrix depends on the eigenvectors of $\boldsymbol{\Phi_e}$, satisfies*

$$e^{2\pi\hat{B}_e(k_1,k_2)} = \boldsymbol{\Phi}_e \ . \qquad (28)$$

The matrix $\hat{B}_e(k_1,k_2)$ is Hamiltonian, i.e.

$$(\mathbb{E}\hat{B}_e(k_1,k_2))^T = \mathbb{E}\hat{B}_e(k_1,k_2) \ , \qquad (29)$$

and defines a canonical Floquet transformation

$$\mathcal{C}(f;e) = \Phi(f;e)e^{-f\hat{B}_e(k_1,k_2)} \qquad (30)$$

which for $e = 0$ is the identity matrix $\mathcal{C}(f;0) = \mathbb{I}$ if k_1, k_2 satisfy

$$\hat{B}_0(k_1,k_2) = A_0 \quad, \quad A_0 := A(f;0). \qquad (31)$$

15

	L_1					L_2				
μ	λ	Ω_1	Ω_2	k_1	k_2	λ	Ω_1	Ω_2	k_1	k_2
1×10^{-6}	2.5251	2.0818	2.0105	2	2	2.4917	2.0615	1.9897	2	-2
5×10^{-6}	2.5371	2.0892	2.0180	2	2	2.4800	2.0544	1.9824	2	-2
1×10^{-5}	2.5447	2.0938	2.0227	2	2	2.4728	2.0500	1.9779	2	-2
5×10^{-5}	2.5710	2.1099	2.0392	2	2	2.4481	2.0350	1.9626	2	-2
0.0001	2.5877	2.1202	2.0497	2	2	2.4328	2.0258	1.9531	2	-2
0.0003	2.6241	2.1425	2.0726	2	2	2.4005	**2.0063**	1.9332	**2**	-2
0.0005	2.6464	2.1563	2.0867	2	2	2.3812	**1.9947**	1.9213	$\mathbf{-2}$	-2
0.0008	2.6709	2.1714	2.1021	2	2	2.3606	1.9823	1.9086	-2	-2
0.001	2.6840	2.1795	2.1104	2	2	2.3497	1.9758	1.9019	-2	-2
0.005	2.8176	2.2625	2.1954	2	2	2.2441	1.9129	1.8376	-2	-2
0.01	2.9037	2.3166	2.2506	2	2	2.1796	1.8749	1.7987	-2	-2
0.03	3.0917	**2.4355**	2.3721	**2**	2	2.0417	1.7948	1.7168	-2	-2
0.05	3.2054	**2.5081**	**2.4462**	$\mathbf{-3}$	**2**	1.9568	1.7462	1.6673	-2	-2
0.08	3.3258	2.5855	**2.5251**	-3	$\mathbf{-3}$	1.8618	1.6927	1.6128	-2	-2
0.1	3.3879	2.6256	2.5660	-3	-3	1.8095	1.6635	**1.5833**	-2	$\mathbf{-2}$
0.2	3.5927	2.7585	2.7015	-3	-3	1.6048	**1.5526**	**1.4713**	$\mathbf{-2}$	**1**
0.3	3.7053	2.8321	2.7764	-3	-3	1.4419	**1.4680**	1.3871	**1**	1
0.49	3.7832	2.8832	2.8283	-3	-3	1.1696	1.2589	1.2589	1	1

Table 2: Values for k_1 (left) and k_2 (right) defined from Eq. (32), according to the values of Ω_1, Ω_2 numerically computed at both Lagrangian points L_1, L_2 for different values of μ. The transitions in the values of k_1, k_2, occurring when Ω_1, Ω_2 cross half integer values, are highlighted in bold.

Choice of the Logarithm of the monodromy matrix. According to Eq. (28) the matrix $2\pi\hat{B}_e(k_1, k_2)$ is a logarithm of the monodromy matrix $\mathbf{\Phi}_e$ for all the choices of the integers k_1, k_2. For $k_1, k_2 = 0$ the matrix $2\pi\hat{B}_e(k_1, k_2)$ is the principal logarithm, which we do not identify as the more convenient choice. Precisely, we use Eq. (31) to fix the values of k_1, k_2 in order to obtain a close to the identity Floquet transformation. By denoting with $\pm i\Omega_1, \pm i\Omega_2$ the complex eigenvalues of A_0 for a given choice of μ, the values of k_1, k_2 providing $\mathcal{C}(f; 0) = \mathbb{I}$ are:

$$k_j = s_j\Omega_j - \frac{1}{2\pi}\arccos\left[\cos(2\pi\Omega_j)\right] \tag{32}$$

where $s_j = 1$ if $\mod(\Omega_j, 1) \in (0, 1/2)$ while $s_j = -1$ if $\mod(\Omega_j, 1) \in (1/2, 1)$. Therefore we may have bifurcations when, by changing the parameter μ, the eigenvalues Ω_1, Ω_2 cross half-integer values. In Table 2 we report the values of k_1 and k_2 defined from Eq. (32), according to the values of Ω_1, Ω_2 computed at both Lagrangian points L_1, L_2 for different values of μ. The transitions in the values of k_1, k_2, occurring when Ω_1, Ω_2 cross half integer values, are highlighted in bold.

Hereafter we assume that the Floquet transformation $\mathcal{C}(f; e)$ is defined with k_1, k_2 satisfying Eq. (32). In fact, the definition of a close to the identity Floquet transformation is essential in order to compute effectively the Birkhoff transformations which remove from the Hamiltonian the dependence on f up to an higher order $N > 2$: if the Floquet transformation is not close to the identity, the Fourier expansion with respect to f of the transformed Hamiltonian, at any order j, contains a large number of terms of large coefficients, and consequently the computation of the Birkhoff normal forms saturates the computer memory at low normalization orders N.

The Hamiltonian $\tilde{H}$ conjugate to H by $\mathcal{C}(f; e)$. Since the matrix $\mathcal{C}(f; e)$ is symplectic, the Floquet transformation

$$(\mathbf{q}, \mathbf{p}) = \mathcal{C}(f; e)(\tilde{\mathbf{q}}, \tilde{\mathbf{p}}),$$

is canonical and conjugates the non-autonomous Hamiltonian $H(\mathbf{q}, \mathbf{p}, f; e)$ to the non-autonomous Hamiltonian:

$$\tilde{H}(\tilde{\mathbf{q}}, \tilde{\mathbf{p}}, f; e) = \tilde{H}_2(\tilde{\mathbf{q}}, \tilde{\mathbf{p}}; e) + \tilde{H}_3(\tilde{\mathbf{q}}, \tilde{\mathbf{p}}, f; e) + \dots \tag{33}$$

where from standard computations we have:

$$\tilde{H}_2 = \frac{1}{2}\mathbf{y} \cdot (\mathbb{E}^T\hat{B}_e(k_1, k_2))\mathbf{y} \quad, \quad \mathbf{y} = (\tilde{\mathbf{q}}, \tilde{\mathbf{p}})$$

is independent on f, and for $j \geq 3$ we have

$$\tilde{H}_j = H_j(\mathcal{C}(f; e)\mathbf{y}, f; e).$$

Notice that, since the canonical transformation is not autonomous, $\tilde{H}$ is not identified with $H(\mathcal{C}(f; e)\mathbf{y}, f; e)$.

For the explicit computation of the polynomials $\tilde{H}_j$ it is convenient to represent the periodic matrix $\mathcal{C}(f; e)$ as a Fourier expansion:

$$\mathcal{C}(f; e) = \mathbb{I} + \sum_{\nu \in \mathbb{Z}} \mathcal{C}_\nu(e) e^{i\nu f} . \tag{34}$$

For practical purposes the series will be truncated and replaced by a sum over all ν satisfying $|\nu| \leq 2^{\mathcal{N}}$, for some convenient $\mathcal{N}$.

The composition of each monomial of the Fourier-Taylor expansion of H:

$$a_{\nu,m_1,m_2,m_3} e^{i\nu f} q_1^{m_1} q_2^{m_2} q_3^{m_3} \quad , \quad \sum_{i=1}^3 m_i = j \geq 3$$

(a_{ν,m_1,m_2,m_3} is a numerical coefficient depending only on μ, e) with the Floquet transformation, provides a perturbation of

$$a_{\nu,m_1,m_2,m_3} e^{i\nu f} \tilde{q}_1^{m_1} \tilde{q}_2^{m_2} \tilde{q}_3^{m_3}$$

which is represented as a Fourier–Taylor expansion of terms:

$$c_{\tilde\nu,\tilde{m},\tilde{n}}(e) \, e^{i\tilde\nu f} \, \tilde{q}_1^{\tilde{m}_1} \tilde{q}_2^{\tilde{m}_2} \tilde{q}_3^{\tilde{m}_3} \tilde{p}_1^{\tilde{n}_1} \tilde{p}_2^{\tilde{n}_2} \tilde{p}_3^{\tilde{n}_3} \quad , \quad \sum_{i=1}^3 (\tilde{m}_i + \tilde{n}_i) = j , \tag{35}$$

where the coefficient $c_{\tilde\nu,\tilde{m},\tilde{n}}(e)$ is proportional to a product of $k \in [1, \ldots, j]$ entries of the matrices $\mathcal{C}_{\nu^\star}(e)$ (with suitable $\nu^\star \in \mathbb{Z}$).

Therefore, the Floquet Transformation increases significantly the Fourier-Taylor expansion of the Hamiltonian. Since the convergence radius of Birkhoff transformations depend not only on the resonance properties of the linear frequencies, but also on the amplitudes of the coefficients of the terms (35) of the Fourier-Taylor expansion of the Hamiltonian, it is convenient to select a Floquet transformation which is close to the identity, so that in all these terms the coefficients $c_{\tilde\nu,\tilde{m},\tilde{n}}(e)$ are small for small values of the eccentricity. This property improves also the efficiency of the numerical computations of the Floquet-Birkhoff normal forms with a computer algebra system, since terms whose amplitude are smaller than a threshold representing the numerical precision, are neglected.

Proof of Lemma. From elementary linear algebra there exists a real symplectic matrix C conjugating the monodromy matrix $\mathbf{\Phi_e}$ to the matrix

$$\tilde{\mathbf{\Phi}}_{\mathbf{e}} := C^{-1} \mathbf{\Phi_e} C = \begin{pmatrix} a_1 & 0 & 0 & \pm b_1 & 0 & 0 \\ 0 & a_2 & 0 & 0 & \pm b_2 & 0 \\ 0 & 0 & e^{\pm 2\pi\lambda} & 0 & 0 & 0 \\ \mp b_1 & 0 & 0 & a_1 & 0 & 0 \\ 0 & \mp b_2 & 0 & 0 & a_2 & 0 \\ 0 & 0 & 0 & 0 & 0 & e^{\mp 2\pi\lambda} \end{pmatrix} . \tag{36}$$

18

The matrix C as well as the signs in (36) are explicitly determined by the eigenvectors of $\Phi_{\mathbf{e}}$. Let ω_1, ω_2 be defined as in (27), and consider the matrix

$$\tilde{B}(k_1, k_2) = \begin{pmatrix} 0 & 0 & 0 & \pm(\omega_1 + k_1) & 0 & 0 \\ 0 & 0 & 0 & 0 & \pm(\omega_2 + k_2) & 0 \\ 0 & 0 & \pm\lambda & 0 & 0 & 0 \\ \mp(\omega_1 + k_1) & 0 & 0 & 0 & 0 & 0 \\ 0 & \mp(\omega_2 + k_2) & 0 & 0 & 0 & 0 \\ 0 & 0 & 0 & 0 & 0 & \mp\lambda \end{pmatrix}$$

where k_1, k_2 are arbitrary integer numbers, and the choice of the signs is done according to the signs appearing in (36). We have

$$\mathrm{e}^{2\pi\tilde{B}(k_1, k_2)} = \tilde{\Phi}_{\mathbf{e}} \ .$$

Finally, since $\hat{B}(k_1, k_2) = C\tilde{B}(k_1, k_2)C^{-1}$ we obtain

$$\mathrm{e}^{2\pi\hat{B}(k_1, k_2)} = \mathrm{e}^{2\pi C\tilde{B}(k_1, k_2)C^{-1}} = C\mathrm{e}^{2\pi\tilde{B}(k_1, k_2)}C^{-1} = \Phi_{\mathbf{e}}$$

thus proving Eq. (26). Equation (29) as well as the symplecticity of the Floquet transformation $\mathcal{C}(f; e)$ follow from elementary algebra. Finally, if $\hat{B}_0(k_1, k_2) = A_0$, we have

$$\mathcal{C}(f; 0) = \mathrm{e}^{fA_0}\mathrm{e}^{-f\hat{B}_0(k_1, k_2)} = \mathbb{I} \ .$$

3.2   The Birkhoff transformations

Let us consider the Hamiltonian:

$$\tilde{H}(\tilde{\mathbf{q}}, \tilde{\mathbf{p}}, f; e) = \tilde{H}_2(\tilde{\mathbf{q}}, \tilde{\mathbf{p}}; e) + \tilde{H}_3(\tilde{\mathbf{q}}, \tilde{\mathbf{p}}, f; e) + \dots \tag{37}$$

where each term $\tilde{H}_j$ is polynomial of degree j in the variables $\tilde{\mathbf{q}}, \tilde{\mathbf{p}}$ and periodic in f with period 2π, conjugate to Hamiltonian (12) by the Floquet transformation. We further apply the linear canonical transformation

$$(\tilde{\mathbf{q}}, \tilde{\mathbf{p}}) = \mathcal{D}(\hat{\mathbf{Q}}, \hat{\mathbf{P}}) \tag{38}$$

conjugating $\tilde{H}_2(\tilde{\mathbf{q}}, \tilde{\mathbf{p}}; e)$ to the function k_2 defined in Eq. (18) (with $\sigma_1 = \pm(\omega_1 + k_1), \sigma_2 = \pm(\omega_2 + k_2)$ defined according to the eigenvalues and eigenvectors of the monodromy matrix $\Phi_{\mathbf{e}}$ as explained in Subsection 3.1) and we introduce the Birkhoff complex canonical variables

$$(\hat{\mathbf{Q}}, \hat{\mathbf{P}}) = \hat{\mathcal{D}}(\hat{\mathbf{q}}, \hat{\mathbf{p}}) \tag{39}$$

defined by

$$\hat{Q}_3 = \hat{q}_3 \ , \quad \hat{P}_3 = \hat{p}_3 \ , \quad \hat{Q}_j = \frac{\hat{q}_j + \mathrm{i}\,\hat{p}_j}{\sqrt{2}} \ , \quad \hat{P}_j = \frac{\mathrm{i}\,\hat{q}_j + \hat{p}_j}{\sqrt{2}} \ , \ j = 1, 2,$$

conjugating $k_2(\hat{\mathbf{Q}}, \hat{\mathbf{P}})$ to

$$\hat{H}_2(\hat{\mathbf{q}}, \hat{\mathbf{p}}) = \mathrm{i}\,\sigma_1\,\hat{q}_1\hat{p}_1 + \mathrm{i}\,\sigma_2\,\hat{q}_2\hat{p}_2 + \lambda\,\hat{q}_3\hat{p}_3. \tag{40}$$

The two linear transformations conjugate the Hamiltonian $\tilde{H}(\tilde{\mathbf{q}}, \tilde{\mathbf{p}}, f; e)$ to

$$\hat{H}(\hat{\mathbf{q}}, \hat{\mathbf{p}}, F, f) = F + \hat{H}_2(\hat{\mathbf{q}}, \hat{\mathbf{p}}) + \sum_{j=1} \hat{H}_j(\hat{\mathbf{q}}, \hat{\mathbf{p}}, f; e) \ , \qquad (41)$$

where the variable F, conjugate to f, has been introduced in order to conveniently deal with an autonomous Hamiltonian and the terms $\hat{H}_j$ for $j \geq 3$ are polynomials of degree j in the variables $\hat{\mathbf{q}}, \hat{\mathbf{p}}$ and periodic in f with period 2π. The terms $\hat{H}_j$ with $j \geq 3$ are represented as sum of monomials of the form

$$a^{(j)}_{\nu, m_1, m_2, m_3, l_1, l_2, l_3} \mathrm{e}^{i\nu f} \hat{q}_1^{m_1} \hat{q}_2^{m_2} \hat{q}_3^{m_3} \hat{p}_1^{l_1} \hat{p}_2^{l_2} \hat{p}_3^{l_3} \ , \quad \sum_{i=1}^{3}(m_i + l_i) = j \ . \qquad (42)$$

Our objective now is twofold: on one hand, we aim to uncouple the hyperbolic variables $\hat{q}_3, \hat{p}_3$ from the elliptic variables $\hat{q}_1, \hat{p}_1$ and $\hat{q}_2, \hat{p}_2$ and, simultaneously, to remove the explicit dependence of $\hat{H}$ on f up to any arbitrary finite order N. This is achieved if σ_1, σ_2 satisfy the non-resonance conditions:

$$j_1\sigma_1 + j_2\sigma_2 + j_3 \neq 0 \quad \forall(j_1, j_2, j_3) \in \mathbb{Z}^3 : \ \ |j_1| + |j_2| \in [1, N], \ \ j_3 \in \mathbb{Z},$$

with a close to the identity canonical transformation $\mathcal{C}_N$ conjugating the Hamiltonian (41), that now we identify as the initial Hamiltonian $\hat{H}^{(2)}$, to a normal form Hamiltonian

$$\hat{H}^{(N)} = F + \sum_{j=2}^{N} K_j^{(N)}(\hat{\mathbf{q}}, \hat{\mathbf{p}}) + \sum_{j \geq N+1} \hat{H}_j^{(N)}(\hat{\mathbf{q}}, \hat{\mathbf{p}}, f) \qquad (43)$$

where $K_j^{(N)}$ do not depend on F, f and are polynomials of degree j depending on $\hat{\mathbf{q}}, \hat{\mathbf{p}}$ only through the products $\hat{q}_1\hat{p}_1, \hat{q}_2\hat{p}_2, \hat{q}_3\hat{p}_3$, while $\hat{H}_j^{(N)}$ are polynomials of degree j with coefficients depending periodically on f with period 2π.

The canonical transformation $\mathcal{C}_N$ is constructed from the composition of a sequence of $N - 2$ elementary canonical Birkhoff transformations. Precisely, we define the sequence of canonical transformations:

$$\mathcal{C}_J = \mathcal{C}_{\chi_J} \circ \mathcal{C}_{J-1} \ , \quad J = 3, \ldots, N \qquad (44)$$

conjugating $\hat{H} := \hat{H}^{(2)}$ to the intermediate Floquet-Birkhoff normal form Hamiltonians:

$$\hat{H}^{(J)} := \hat{H}^{(J-1)} \circ \mathcal{C}_J = F + \sum_{j=2}^{J} K_j^{(J)}(\hat{\mathbf{q}}, \hat{\mathbf{p}}) + \sum_{j \geq J+1} \hat{H}_j^{(J)}(\hat{\mathbf{q}}, \hat{\mathbf{p}}, f) \qquad (45)$$

with the property that $K_j^{(J)}$ do not depend on F, f and are polynomials of degree j depending on $\hat{\mathbf{q}}, \hat{\mathbf{p}}$ only through the products $\hat{q}_1\hat{p}_1, \hat{q}_2\hat{p}_2, \hat{q}_3\hat{p}_3$, while $\hat{H}_j^{(J)}$ are polynomials of degree j with coefficients depending periodically on f with period 2π.

The transformation $\mathcal{C}_2$ is the identity while $\mathcal{C}_{\chi_J}$ is the Hamiltonian flow at time $f = 1$ of suitable generating functions χ_J defined from the coefficients of $\hat{H}^{(J-1)}$. Below we describe

the definition of the generating functions χ_J and the steps required for the algorithmic computation of each canonical transformation $\mathcal{C}_N$ and Hamiltonian $\hat{H}^{(N)}$ using the Lie series method (for an introduction to the method, see [10, 14]) and implemented with a computer algebra system in the examples presented in this paper. We remark that, when using a computer algebra system, we need to set a cut off on the Fourier expansions with respect to the periodic variable f.

For each $J \geq 3$ we assume that the Hamiltonian $\hat{H}^{(J-1)}$ and the canonical transformation $\mathcal{C}_{N-1}$ are known, and we proceed as follows.

First, from $\hat{H}^{(J-1)}$ we compute the generating function χ_J:

$$\chi_J = \sum_{\substack{m_j, l_j \in \mathbb{N}: \\ \sum_n (m_n + l_n) = N, \\ m_1 \neq l_1 \vee m_2 \neq l_2 \vee \\ m_3 \neq l_3 \vee \nu \neq 0}} \frac{-a^{(J-1)}_{\nu, m_1, m_2, m_3, l_1, l_2, l_3}}{i\,\sigma_1(l_1 - m_1) + i\,\sigma_2(l_2 - m_2) + \lambda\,(l_3 - m_3) + i\,\nu}\, e^{i\nu f}\, \hat{q}_1^{m_1} \hat{q}_2^{m_2} \hat{q}_3^{m_3} \hat{p}_1^{l_1} \hat{p}_2^{l_2} \hat{p}_3^{l_3}.$$

(46)

Next, we compute the canonical transformation

$$\mathcal{C}_{\chi_J}(\hat{\mathbf{q}}^{(J)}, \hat{\mathbf{p}}^{(J)}, F^{(J)}, f^{(J)}) = (\hat{\mathbf{q}}^{(J-1)}, \hat{\mathbf{p}}^{(J-1)}, F^{(J-1)}, f^{(J-1)}) \,,$$

defined by the Hamiltonian flow of the generating function χ_J at time $f = 1$. The transformation $\mathcal{C}_{\chi_J}$ is explicitly represented as the Lie series

$$\zeta = e^{L_{\chi_J}} \zeta' := \zeta' + \{\zeta', \chi_J\} + \frac{1}{2}\{\{\zeta', \chi_J\}, \chi_J\} + \dots \,,$$

(47)

where $L_{\chi_J} := \{\cdot, \chi_J\}$, and ζ, ζ' denote any couple of variables $\hat{\mathbf{q}}^{(J-1)}, \hat{\mathbf{q}}^{(J)}, \hat{\mathbf{p}}^{(J-1)}, \hat{\mathbf{p}}^{(J)}$ or $F^{(J-1)}, F^{(J)}$ respectively. The transformed Hamiltonian is computed as a Lie series as well:

$$\hat{H}^{(J)} = \mathcal{C}_{\chi_J}\, \hat{H}^{(J-1)} = e^{L_{\chi_J}}\, \hat{H}^{(J-1)}.$$

(48)

The iteration ends for $J = N$, and finally, by reintroducing real canonical variables,

$$\begin{aligned}
\hat{q}_1^{(N)} &= \frac{Q_1 - i\,P_1}{\sqrt{2}} \,, & \hat{p}_1^{(N)} &= \frac{P_1 - i\,Q_1}{\sqrt{2}} \,, \\
\hat{q}_2^{(N)} &= \frac{Q_2 - i\,P_2}{\sqrt{2}} \,, & \hat{p}_2^{(N)} &= \frac{P_2 - i\,Q_2}{\sqrt{2}} \,, \\
\hat{q}_3^{(N)} &= Q_3 \,, & \hat{p}_3^{(N)} &= P_3 \,,
\end{aligned}$$

(49)

and by suitably identifying the terms k_j with K_j, and disregarding the dummy action $F^{(N)}$, we recover the final Floquet-Birkhoff normal form as in Eq. (6) or (15).

4 Experiments and examples

4.1 On the numerical computation of the Floquet-Birkhoff normal form

In Section 3 we defined the Floquet-Birkhoff normal forms in the neighbourhood of a collinear equilibrium point of the ERTBP. For given values of the parameters μ, e the Floquet-Birkhoff normal forms can be numerically provided as a Fourier-Taylor expansions:

$$a_{\nu, m_1, m_2, m_3} e^{|\nu|} \mathrm{e}^{i\nu f} q_1^{m_1} q_2^{m_2} q_3^{m_3} \quad , \quad \sum_{i=1}^{3} m_i = j \geq 3$$

where the coefficients a_{ν, m_1, m_2, m_3} are floating point numbers. All the steps required to compute the Floquet-Birkhoff normal form are explicit algebraic operations which can be implemented with a computer algebra system. The only exception is the computation of the principal fundamental matrix which demands the numerical integration of a non-autonomous ODE.

In the present Subsection we provide an example of computation of the Floquet-Birkhoff normal form in a neighbourhood of the Lagrangian point L_1 of the Earth-Moon ERTBP defined by $\mu = 0.0123$ and $e = 0.0549006$; correspondingly we have $\beta = 2.5764...$ (see Eq. (14)). The input Hamiltonian system is Hamiltonian (3) explicitly computed as a Taylor expansion in the variables $(\mathbf{q}, \mathbf{p})$ up the polynomial order $N_{tot} = N + N_r$, where N is the order of the Floquet-Birkhoff normal form, and $N_r \geq 1$ is needed to compute the lowest orders of the remainder. The examples below are computed for $N = 8$ and $N_r = 2$.

4.1.1 Computation of the canonical Floquet transformation $\mathcal{C}(f; e)$

Numerical computation of the principal fundamental matrix solution. The principal fundamental matrix solution $\Phi(f; e)$ of the linear differential equation defined by the Hamilton equations of H_2 (see Eq. (13)):

$$\begin{pmatrix} \dot{\mathbf{q}} \\ \dot{\mathbf{p}} \end{pmatrix} = A(f; e) \begin{pmatrix} \mathbf{q} \\ \mathbf{p} \end{pmatrix} \tag{50}$$

can be provided as a Fourier series in the variable f with floating point coefficients, as it was done in [32]. The computation requires the numerical integration of (50) with six different initial conditions identified with the vectors $\mathbf{u}^{(i)} \in \mathbb{R}^6$ of the standard basis of $\mathbb{R}^6$. Next, we apply the Fast Fourier Transform algorithm on the outputs $\mathbf{u}^{(i)}(f)$ sampled on a regular grid of values of

$$f = f_j := 2\pi \frac{j}{2^{\mathcal{N}}} \quad , \quad j = 1, \ldots, 2^{\mathcal{N}} \quad ,$$

where the value of $\mathcal{N} \in \mathbb{N}$ sets the Fourier cut-off in the variable f.

The implementation of these numerical procedures to the collinear Lagrangian points L_1, L_2 requires a careful check of the numerical precision, since the partially hyperbolic

nature of these equilibrium points determines an exponential loss of the numerical precision in the integration of the initial conditions which may be responsible of large errors in the computation of the matrices $\Phi(f_j; e)$. For example, we find that the monodromy matrix $\mathbf{\Phi_e}$ has large entries of order 10^8, and the characteristic polynomial $\det[\Phi_e - \lambda \mathcal{I}]$ has coefficients separated by 8 orders of magnitude. To check the precision of the computation:

– We perform the numerical integration of the linear equation (50) with an explicit Runge-Kutta of order six, quadruple floating point precision and integration step $h = 1 \times 10^{-4} \pi$. In order to check the precision of our result we extend the computation over the larger interval $[0, 4\pi]$.

– To prevent unnecessary loss of precision digits due to the strong amplification of the norm of the solution vectors during the computation, we normalize the solution vector $\mathbf{x} = (\mathbf{q}, \mathbf{p})$ every time its norm surpasses a certain threshold ρ, and we store in the computer memory the quantity $\|\mathbf{x}\|$; we continue the computation with the vector $\mathbf{x}/\|\mathbf{x}\|$. The threshold on the norm of the solution vector that we used was $\rho = 1 \times 10^3$. Since the differential equation is linear, we reconstruct the solution $\mathbf{x}(f)$ by suitably multiplying the normalized solutions with the normalizing factors. This is the technique introduced in [3] for the precise numerical computation of the Lyapunov exponents.

– Since the linear equation (50) is periodic in f of period 2π, we check the precision of the numerical computation by checking if the eigenvalues of $\Phi(4\pi; e)$ are the square of the eigenvalues of $\Phi(2\pi; e)$.

Finally, the entries of the matrices $\Phi(f_j; e)$ are defined by

$$\Phi(f_j; e)_{ki} = u_k^{(i)}(f_j).$$

The experiments described below have been performed with $\mathcal{N} = 5$; we obtained (we here report only few precision digits):

$$\mathbf{\Phi_e} = \begin{pmatrix} 5.339 \times 10^7 & 5.646 \times 10^6 & 0 & 1.632 \times 10^7 & 7.725 \times 10^6 & 0 \\ -2.556 \times 10^7 & -2.673 \times 10^6 & 0 & -7.725 \times 10^6 & -3.657 \times 10^6 & 0 \\ 0 & 0 & -0.13223 & 0 & 0 & 0.44660 \\ 1.787 \times 10^8 & 1.868 \times 10^7 & 0 & 5.399 \times 10^7 & 2.556 \times 10^7 & 0 \\ -1.868 \times 10^7 & -1.953 \times 10^6 & 0 & -5.646 \times 10^6 & -2.673 \times 10^6 & 0 \\ 0 & 0 & -2.19997 & 0 & 0 & -0.13223 \end{pmatrix},$$

whose eigenvalues are $e^{(2\pi\lambda)} = 1.02644...\times 10^8$, $e^{-(2\pi\lambda)} = 9.74245...\times 10^{-9}$, with $\lambda \sim 2.935896...$, $a_1 \pm i\, b_1 = -0.51780296... \pm i\, 0.8554999...$ and $a_2 \pm ib_2 = -0.132227... \pm i\, 0.9912195....$

Choice of a logarithm of $\mathbf{\Phi_e}$. The algebraic Lemma of Section 3 provides a family of matrices $\hat{B}_e(k_1, k_2)$ such that, for any choice of the integers k_1, k_2 the matrix $2\pi \hat{B}_e(k_1, k_2)$ is a logarithm of the monodromy matrix $\mathbf{\Phi_e}$. As already remarked in Section 3, in order to obtain a close to the identity Floquet transformation we chose $(k_1, k_2) = (2, 2)$ according

to Eq. (32), with $\Omega_1 = 2.335547...$, $\Omega_2 = 2.270018...$ eigenvalues of the matrix A_0 (see Eq. (25)). From Eq. (26) we have:

$$\hat{B}_e(2,2) = \begin{pmatrix} 0 & 1.02669 & 0 & 1.03421 & 0 & 0 \\ -1.03717 & 0 & 0 & 0 & 1.01949 & 0 \\ 0 & 0 & 0 & 0 & 0 & 1.02327 \\ 10.0729 & 0 & 0 & 0 & 1.03717 & 0 \\ 0 & -5.03017 & 0 & -1.02669 & 0 & 0 \\ 0 & 0 & -5.04063 & 0 & 0 & 0 \end{pmatrix}.$$

The Fourier series of $\mathcal{C}(f,e)$. From Eq. (21) we obtain a sample of the matrix $\mathcal{C}(f,e)$:

$$C_j := \mathcal{C}(f_j, e) = \Phi(f_j, e)\, e^{-\hat{B}_e(2,2,)\, f_j}\ , \quad j = 0, \ldots, 2\pi \tag{51}$$

which we use to compute a Fourier series for $\mathcal{C}(f,e)$, using the Fast Fourier Transform algorithm. Precisely, by denoting with $C_j^{(l,m)}$ the entries of C_j, the FFT algorithm gives

$$v_s^{(l,m)} = \frac{1}{\sqrt{2^{\mathcal{N}}}} \sum_{r=1}^{2^{\mathcal{N}}} C_r^{(l,m)} e^{2\pi\, i(r-1)(s-1)/2^{\mathcal{N}}}\ ,$$

which provide the Fourier representation:

$$\mathcal{C}^{(l,m)}(f,e) = \frac{1}{\sqrt{2^{\mathcal{N}}}} \sum_{s=0}^{2^{\mathcal{N}-1}-1} v_{s+1}^{(l,m)} e^{-is f} \frac{1}{\sqrt{2^{\mathcal{N}}}} + \sum_{s=2^{\mathcal{N}-1}}^{2^{\mathcal{N}}-1} v_{s+1}^{(l,m)} e^{-i(s-2^{\mathcal{N}})f}\ . \tag{52}$$

In Figure 5 we plot a comparison between the values of $C^{(1,2)}(f,e)$, computed using Eq. (21), and the values of the Fourier series compute using Eq. (21) on a random sample of values of f; we appreciate that also for $f \neq f_j$ the difference sums to order 10^{-19}. This number is in agreement with the decay of the values of the coefficients $v_\nu^{(l,m)}$, where the stabilization of the values of $|v_\nu^{(l,m)}|$ at 10^{-19} for the largest ν provides an indication that the numerical error is 10^{-19}. The improvement of this threshold value requires to increase the value of the Fourier cut-off and to increase the numerical precision of the floating point arithmetics as well as of the numerical integration of Eq. (50).

Computation of the Fourier-Taylor expansion $\tilde{H}(\tilde{\mathbf{q}}, \tilde{\mathbf{p}}, f; e)$. The canonical Floquet transformation conjugates the Hamiltonian $H(\mathbf{q}, \mathbf{p}, f; e)$ to the Hamiltonian $\tilde{H}(\tilde{\mathbf{q}}, \tilde{\mathbf{p}}, f; e)$. Since the Fourier decomposition of the $\mathcal{C}(f,e)$ is limited to the Fourier cut-off $2^{\mathcal{N}-1}$, we preliminary compute the Taylor-Fourier expansion of $H(\mathbf{q}, \mathbf{p}, f; e)$ by expanding the function

$$\frac{1}{1 + e \cos f} = \sum_{\nu \in \mathbb{Z}} \alpha_\nu e^{i\nu f}$$

and by limiting the expansion to the Fourier cut-off $2^{\mathcal{N}-1}$. The ultra-violet part of the Hamiltonian $H(\mathbf{q}, \mathbf{p}, f; e)$ will be neglected. The second order term of the expansion is:

$$\begin{aligned} \tilde{H}_2(\tilde{\mathbf{q}}, \tilde{\mathbf{p}}; e) =\ & 0.517196\, \tilde{p}_1{}^2 + 0.509743\, \tilde{p}_2{}^2 + 0.511635\, \tilde{p}_3{}^2 - 1.03717\, \tilde{p}_2\, \tilde{q}_1 \\ & + 1.02669\, \tilde{p}_1\, \tilde{q}_2 - 5.03647 \tilde{q}_1{}^2 + 2.51509\, \tilde{q}_2{}^2 + 2.52031\, \tilde{q}_3{}^2 \end{aligned} \tag{53}$$

24
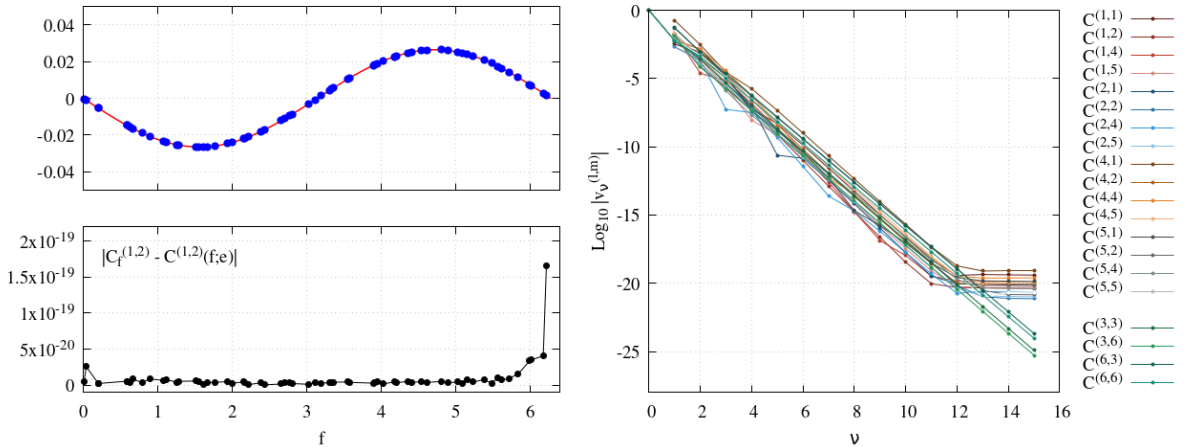
Figure 5: Top left panel: comparison between the analytic expression for $\mathcal{C}^{(1,2)}(f,e)$ provided by Eq. (21) (red line) and its Fourier expansion provided by Eq. (52) computed on a random sample of values of f (blue dots). In the bottom left panel we represent the absolute value of the difference between the analytic expression for $\mathcal{C}^{(1,2)}(f,e)$ and the value of its Fourier expansion. In the right panel we provide all the values of $|v_\nu^{(l,m)}|$ appearing in the Fourier representations Eq. (52) versus ν.

while the higher order terms $\tilde{H}_j$ are polynomials with coefficients expanded as a Fourier series of f with Fourier cut-off $2^{\mathcal{N}-1}$.

4.1.2 Computation of the second-order normal form

To compute the linear canonical transformations (17) and (39) conjugating the second order Hamiltonian $\tilde{H}_2$ in (53) to its normal form (40) we proceed as usual by considering the matrix $A = \mathbb{E}\nabla\tilde{H}_2$, and by computing its eigenvalues $\pm\mathrm{i}\sigma_1 = \pm\mathrm{i}\,2.336625$, $\pm\mathrm{i}\sigma_2 = \pm\mathrm{i}\,2.271106$, $\pm\lambda = \pm 2.935895$, and the associated eigenvectors $v_{-\sigma_1}, v_{\sigma_1}, v_{-\sigma_2}, v_{\sigma_2} \in \mathbb{C}^6$, $v_{-\lambda}, v_\lambda \in \mathbb{R}^6$. Then, we compute the coefficients c_1, c_2, c_3 such that the matrix

$$\mathcal{D}_0 = (c_1 v_{\sigma_1}, c_2 v_{\sigma_2}, c_3 v_\lambda, \mathrm{i}\,c_1 v_{-\sigma_1}, \mathrm{i}\,c_2 v_{-\sigma_2}, c_3 v_{-\lambda})$$

(i.e. the first column of $\mathcal{D}_0$ is the vector $c_1 v_{\sigma_1}$, etc.) is symplectic. The linear transformation

$$\begin{pmatrix} \tilde{\mathbf{q}} \\ \tilde{\mathbf{p}} \end{pmatrix} = \mathcal{D}_0 \begin{pmatrix} \hat{\mathbf{q}} \\ \hat{\mathbf{p}} \end{pmatrix} \tag{54}$$

is canonical and conjugates the second order Hamiltonian $\tilde{H}_2$ in (53) to the second order normal form

$$\hat{H}_2(\hat{\mathbf{q}}, \hat{\mathbf{p}}) = 2.336625\,\mathrm{i}\,\hat{q}_1\hat{p}_1 + 2.271106\,\mathrm{i}\,\hat{q}_2\hat{p}_2 + 2.935895\,\hat{q}_3\hat{p}_3 \,. \tag{55}$$

25

and for $j \geq 3$ the terms $\tilde{H}_j$ to polynomials $\hat{H}_j$ of degree j, whose coefficients are periodic in f and expanded as Fourier series with cut-off $2^{\mathcal{N}-1}$. The Hamiltonian:

$$\hat{H}(\hat{\mathbf{q}}, \hat{\mathbf{p}}, f, F; e) = F + \hat{H}_2(\hat{\mathbf{q}}, \hat{\mathbf{p}}) + \sum_{j=1}^{N_{tot}} \hat{H}_j(\hat{\mathbf{q}}, \hat{\mathbf{p}}, f; e) \ , \tag{56}$$

where the variable F, conjugate to f, has been introduced in order to conveniently deal with an autonomous Hamiltonian, is the input of the Birkhoff normalization algorithm defined in Subsection 3.2.

4.1.3 The Floquet-Birkhoff normal form

The Birkhoff normalization can be implemented if for the specific values of μ, e there are no resonances:

$$j_1 \sigma_1 + j_2 \sigma_2 + j_3 \neq 0 \quad \forall (j_1, j_2) \in \mathbb{Z}^3 : |j_1| + |j_2| \in [1, N], \forall j_3 \in \mathbb{Z}$$

of order smaller or equal than $N = 3$. For the values of μ, e indicated previously, we provide the details of the computation of the Floquet-Birkhoff normal form of order $N = 8$, by performing $N - 2 = 6$ Birkhoff transformations defined in Subsection 3.2. Since the computation of the Birkhoff transformations and of all the intermediate Hamiltonians using the Lie series method are fully described in Subsection 3.2, we here report the results. We find that the Floquet-Birkhoff normal form Hamiltonian of order 8 is given by

$$\hat{H}^{(8)} = F + \sum_{j=1}^{J/2} K_{2j}^{(8)}(\hat{\mathbf{q}}, \hat{\mathbf{p}}) + \sum_{j \geq 9} \hat{H}_j^{(8)}(\hat{\mathbf{q}}, \hat{\mathbf{p}}, f) \tag{57}$$

where:

$$\begin{aligned}
K_2^{(8)}(\hat{\mathbf{q}}, \hat{\mathbf{p}}) =& \hat{H}_2(\hat{\mathbf{q}}, \hat{\mathbf{p}}) = 2.336625 \, \mathrm{i} \, \hat{q}_1 \, \hat{p}_1 + 2.271106 \, \mathrm{i} \, \hat{q}_2 \, \hat{p}_2 + 2.935895 \, \hat{q}_3 \, \hat{p}_3 \\
K_4^{(8)}(\hat{\mathbf{q}}, \hat{\mathbf{p}}) =& 7.076324 \, \hat{q}_1^2 \, \hat{p}_1^2 + 3.187254 \, \hat{q}_1 \, \hat{p}_1 \, \hat{q}_2 \, \hat{p}_2 + 6.326523 \, \hat{q}_2^2 \, \hat{p}_2^2 \\
& - 32.88244 \, \mathrm{i} \, \hat{q}_1 \, \hat{p}_1 \, \hat{q}_3 \, \hat{p}_3 - 30.07314 \, \mathrm{i} \, \hat{q}_2 \, \hat{p}_2 \, \hat{q}_3 \, \hat{p}_3 - 9.578629 \, \hat{q}_3^2 \, \hat{p}_3^2
\end{aligned}$$

and the coefficients of $K_6^{(8)}, K_8^{(8)}$ are reported in Table 3 ($K_j^{(8)}$ do not depend on F, f and are polynomials of degree j depending on $\hat{\mathbf{q}}, \hat{\mathbf{p}}$ only through the products $\hat{q}_1 \hat{p}_1, \hat{q}_2 \hat{p}_2, \hat{q}_3 \hat{p}_3$; the notations of Table 3 is in agreement with Eq. (42)).

The terms denoted with $\sum_{j \geq 9} \hat{H}_j^{(8)}$ are explicitly computed for $j = 9, 10$, and are referred below as the remainder of the Floquet-Birkhoff normal form. We find 97233 terms in in the remainder with coefficients larger than 10^{-16}.

Figure 6 provides a snapshot of the decay of the Fourier harmonics $a_{\nu, m_1, m_2, m_3, l_1, l_2, l_3}^{(j)}$ with ν (see Eq. (42)). The exponential decay of the harmonics with the label ν appears clearly. As it is typical of Birkhoff normal form remainders, the absolute values of the coefficients increase with the order j, so that the convergence of the remainder must be checked in neighbourhoods $(\hat{\mathbf{q}}, \hat{\mathbf{p}}) = (0, 0)$. As a consequence, we compute the maximum value of the norm of the remainder along bounded orbits of the planar and of the spatial

problems. The choice of the initial conditions is done in the normalized variables $(\hat{\mathbf{q}}, \hat{\mathbf{p}})$ of the Floquet-Birkhoff normal form (56) of order $N = 8$. Precisely, we consider the 4 sets of points $(\hat{\mathbf{q}}, \hat{\mathbf{p}}, f)$ in the planar two-dimensional tori $\mathcal{M}_{I_B,0}$, $\mathcal{M}_{I_R,0}$ (the sets *i,ii*) and in the fully spatial two-dimensional tori $\mathcal{M}_{0,I_G}$, $\mathcal{M}_{0,I_P}$ (the sets *iii, iv*); the colors refer to Figure 7:

i. Blue points: $\hat{q}_1 = -\mathrm{i}\sqrt{I_B}\,\mathrm{e}^{\mathrm{i}\phi}$, $\hat{p}_1 = \sqrt{I_B}\,\mathrm{e}^{\mathrm{i}\phi}$, with $I_B = 1{\times}10^{-5}$ and $\phi = j(2\pi/20)$, $f = i(2\pi/5)$, $j = 1, 20$, $i = 1, 5$; $\hat{q}_2 = \hat{p}_2 = \hat{q}_3 = \hat{p}_3 = 0$, $\kappa_B = \hat{\mathcal{K}}(I_B, 0, 0) \approx 2.33655{\times}10^{-5}$.

ii. Red points: $\hat{q}_1 = -\mathrm{i}\sqrt{I_R}\,\mathrm{e}^{\mathrm{i}\phi}$, $\hat{p}_1 = \sqrt{I_R}\,\mathrm{e}^{\mathrm{i}\phi}$, with $I_R = 1{\times}10^{-4}$ and with $\phi = j(2\pi/20)$, $f = i(2\pi/5)$, $j = 1, 20$, $i = 1, 5$; $\hat{q}_2 = \hat{p}_2 = \hat{q}_3 = \hat{p}_3 = 0$, $\kappa_R = \hat{\mathcal{K}}(I_R, 0, 0) \approx 2.33655{\times}10^{-4}$.

iii. Green points: $\hat{q}_2 = -\mathrm{i}\sqrt{I_G}\,\mathrm{e}^{\mathrm{i}\phi}$, $\hat{p}_2 = \sqrt{I_G}\,\mathrm{e}^{\mathrm{i}\phi}$, with $I_G = 2{\times}10^{-5}$ and $\phi = j(2\pi/20)$, $f = i(2\pi/5)$, $j = 1, 20$, $i = 1, 5$; $\hat{q}_1 = \hat{p}_2 = \hat{q}_1 = \hat{p}_3 = 0$, $\kappa_G = \hat{\mathcal{K}}(0, I_G, 0) \approx 4.54196{\times}10^{-5}$.

iv. Purple points: $\hat{q}_{20} = -\mathrm{i}\sqrt{I_P}\,\mathrm{e}^{\mathrm{i}\phi}$, $\hat{p}_{20} = \sqrt{I_P}\,\mathrm{e}^{\mathrm{i}\phi}$, with $I_P = 2{\times}10^{-4}$ and $\phi = j(2\pi/20)$, $f = i(2\pi/5)$, $j = 1, 20$, $i = 1, 5$; $\hat{q}_{10} = \hat{p}_{20} = \hat{q}_{10} = \hat{p}_{30} = 0$, $\kappa_P = \hat{\mathcal{K}}(0, I_P, 0) \approx 4.53968{\times}10^{-4}$.
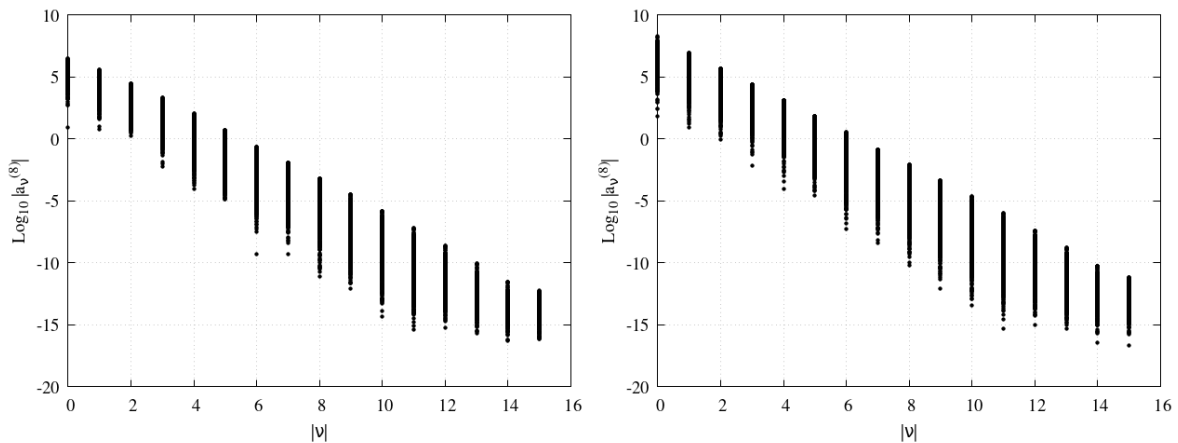
Figure 6: Logarithmic representation of the values of the coefficients $|a^{(8)}_{\nu,m_1,m_2,m_3,l_1,l_2,l_3}|$ appearing in the terms $\hat{H}_9^{(8)}$ (left) and $\hat{H}_{10}^{(8)}$ (right) of the remainder of the Hamiltonian (57): for each value of ν, we plot a dot corresponding to the logarithm of $|a^{(8)}_{\nu,m_1,m_2,m_3,l_1,l_2,l_3}|$ for all the possible values of m_j, l_j.

In Fig. 7, for the four sets of points with the corresponding color, the full orbits are represented in gray.

We compute the maximum of the norm of the remainder:

$$|R^{(J)}| := \mathrm{Max}_{(\hat{\mathbf{q}}, \hat{\mathbf{p}}, f)\in\mathcal{S}} \sum_{j=J+1}^{10} |\hat{H}_j^{(J)}(\hat{\mathbf{q}}, \hat{\mathbf{p}}, f)| \tag{58}$$

where $\mathcal{S}$ represent the sets of points (i), (ii), (iii) or (iv), for all the normalization orders $J = 2, \ldots, 8$. The results are summarized in Table 4, and show the orders of magnitude
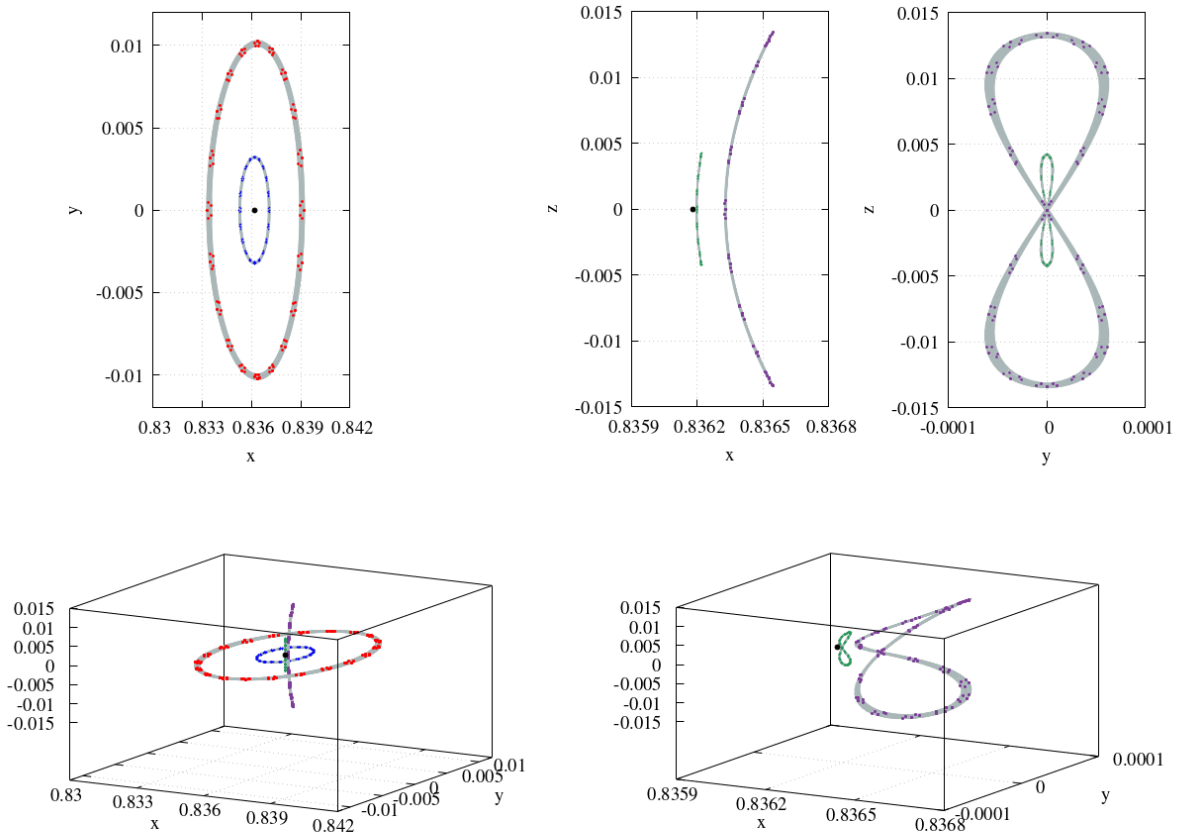
Figure 7: Representation of the points of the orbits used for the estimation of the norm of the remainder in Table 4. The blue and red sets are in the planar two-dimensional tori $\mathcal{M}_{I_B,0}$ and $\mathcal{M}_{I_R,0}$ respectively; the green and purple sets are in the vertical two-dimensional tori $\mathcal{M}_{0,I_G}$, $\mathcal{M}_{0,I_P}$. In all the cases, the complete orbits are represented in gray.

of improvement in the error of our best Floquet-Birkhoff normal form (of order $J = 8$) with respect to the classical Floquet approximation where no Birkhoff transformation are implemented (corresponding to order $J = 2$).

4.2   Computation of transit orbits

An immediate application of the Floquet-Birkhoff normal form is the computation of initial conditions of transit orbits. In this Subsection, we discuss this application in the direction of Figures 1, 2, 3 and 4, already presented in Section 2, where the initial conditions have been chosen using the Floquet-Birkhoff normal form, and the orbits have been obtained by numerically integrating the Hamiltonian (1). These examples refer to the planar problem. As already described in Section 2, for all small values of κ we obtain the initial conditions of transit orbits according to their position with respect to manifold

j	$m_1 = l_1$	$m_2 = l_2$	$m_3 = l_3$	$a^{(8)}_{m_1,m_2,m_3}$
6	3	0	0	$25.117460\,\mathrm{i}$
6	2	1	0	$-782.054619\,\mathrm{i}$
6	1	2	0	$791.940455\,\mathrm{i}$
6	0	2	0	$15.932649\,\mathrm{i}$
6	2	0	1	47.958271
6	1	1	1	223.182838
6	0	2	1	14.202204
6	1	0	2	$-210.843893\,\mathrm{i}$
6	0	1	2	$-141.046741\,\mathrm{i}$
6	0	0	3	-54.461156
8	4	0	0	-101.849178
8	3	1	0	$1.4081041{\times}10^5$
8	2	2	0	$-3.6931581{\times}10^5$
8	1	3	0	$1.0572474{\times}10^5$
8	0	4	0	-12.515592
8	0	3	1	$-289.061089\,\mathrm{i}$
8	2	1	1	$-6.8347427{\times}10^3\,\mathrm{i}$
8	1	2	1	$9.388619{\times}10^3\,\mathrm{i}$
8	0	3	1	$-663.967899\,\mathrm{i}$
8	0	2	2	$-2.088688{\times}10^3$
8	1	1	2	$-4.705106{\times}10^3$
8	0	2	2	$-2.791412{\times}10^3$
8	1	0	3	$-2.607692{\times}10^3\,\mathrm{i}$
8	0	1	3	$-1.057350{\times}10^3\,\mathrm{i}$
8	0	0	4	-558.96388

Table 3: Coefficients and combination of powers appearing in the terms of the normal form (57), for a maximum polynomial expansion of order $N = 8$.

tubes $W^{s,loc}_\kappa, W^{u,loc}_\kappa$, determined by the sign of $\mathcal{I}_3 = Q_3 P_3 > 0$. The transits of Figures 1, 2, 3 and 4 have been computed using the highest order normal form $\hat{H}^{(8)}$ that we have computed, disregarding the remainder terms. The transformations between the Cartesian variables $(\mathbf{q}, \mathbf{p})$ to the final Floquet-Birkhoff variables are computed explicitly up to order 8 as well, and will be denoted below by

$$(\mathbf{Q}, \mathbf{P}) = \Psi^{-1}(\mathbf{q}, \mathbf{p}, f; e) \quad , \quad (\mathbf{q}, \mathbf{p}) = \Psi(\mathbf{Q}, \mathbf{P}, f; e)$$

respectively.

For the planar problem it is more convenient to use the value $\mathcal{I}_1$ of the planar tori defined by $\mathcal{M}_{\mathcal{I}_1,0}$ as an independent choice, for which we compute the value κ of the local energy correspondingly. For that value of κ, we compute in Cartesian coordinates: the planar torus defined by $\mathcal{M}_{\mathcal{I}_1,0}$, i.e.

$$\bigcup_{f,\phi\in[0,2\pi]} \{\Psi(\mathbf{Q}, \mathbf{P}, f; e) : (Q_1, P_1) = \sqrt{2\,\mathcal{I}_1}(\sin\phi, \cos\phi) \ , \ Q_2, P_2, Q_3, P_3 = 0\}, \quad (59)$$

Blue set		Red set	
J	$|R^{(J)}|$	J	$|R^{(j)}|$
2	8.301112×10^{-8}	2	2.779487×10^{-6}
3	1.710948×10^{-9}	3	1.761621×10^{-7}
4	2.212756×10^{-11}	4	7.291894×10^{-9}
5	4.045467×10^{-13}	5	4.224178×10^{-10}
6	7.702234×10^{-15}	6	2.557286×10^{-11}
7	1.646918×10^{-16}	7	1.737068×10^{-12}
8	3.911953×10^{-18}	8	1.292694×10^{-13}
Green set		Purple set	
J	$|R^{(J)}|$	J	$|R^{(J)}|$
2	2.373759×10^{-7}	2	8.139141×10^{-6}
3	6.881388×10^{-9}	3	7.177421×10^{-7}
4	1.261467×10^{-10}	4	4.233325×10^{-8}
5	3.262695×10^{-12}	5	3.473169×10^{-9}
6	8.793931×10^{-14}	6	2.983974×10^{-10}
7	2.661757×10^{-15}	7	2.872606×10^{-11}
8	8.927986×10^{-17}	8	3.001279×10^{-12}

Table 4: Results of the estimation of the norm of the remainder (58) for the four sets of points represented in Fig. 7.

the transit orbits and the zero velocity curves.

As a demonstration, in the panels (a) of Fig. 1 and Fig. 2 we report in pink color a sample of the set (59) computed for $\kappa = 0.0000233655, 0.0000467296, 0.0002335917$ (Fig. 1) and $\kappa = 0.00232952, 0.0115030, 0.0204374$ (Fig. 2); the section of the tori corresponding to $f = 0$ is depicted in black in each case. The initial conditions for the planar transit orbits have been chosen in the normalized variables satisfying $\mathcal{I}_2 = 0$, $\mathcal{I}_3 = Q_3 P_3 > 0$ and $\mathcal{I}_1$ compatible with the fixed value κ of the local energy (see the discussion in Section 2). Once the value of $\mathcal{I}_3$ has been fixed, we choose $|P_3(0)| \gg |Q_3(0)|$, so as to construct initial conditions in the close vicinity of the stable manifold $W_\kappa^{s,loc}$. The transit orbits in Fig. 1 and Fig. 2 have been obtained for $\mathcal{I}_3 = 1. \times 10^{-10}$ and

$$
\begin{aligned}
&Q_1(0) = 0 , && P_1(0) = \sqrt{2\,\mathcal{I}_1} , \\
&Q_2(0) = 0 , && P_2(0) = 0 , \\
&Q_3(0) = \mathcal{I}_3/P_3(0) , && P_3(0) = 1 \times 10^{-4} .
\end{aligned}
\tag{60}
$$

Finally, using the direct transformation $\Psi(\mathbf{Q}, \mathbf{P}, f; e)$ and fixing the value of f, e.g. $f = 0$, the initial condition (60) is mapped in Cartesian variables. In Fig. 1 we show the orbits with these initial conditions, obtained from the numerical integration of the Hamilton's equations of (1). In each case, we also show the corresponding torus (59) and the zero velocity curves, which are obtained by solving numerically Eq. (8), i.e. by computing numerically the level curves of the local energy $\hat{\mathcal{K}}$, approximated at order $N = 8$, for sample values of f. The color scale in the orbits indicates the variation of the local energy

with respect to the initial value, exhibiting the preservation of the local energy during the whole transition. We notice that for the largest value of κ, as soon as the transit orbit quits a neighbourhood of the torus (59), it reaches distances from the Lagrangian point comparable to the distance of L_1 to P_2. In [37] we have shown that at these distances the normal forms computed using the Cartesian variables looses convergence, due to the gravitational singularity represented by P_2. Therefore we do not represent the zero velocity curves in this case, since only very close to the torus (59) we expect a good conservation of the local energy. As visual reference, we have included in this panel the zero velocity curve obtained from the Circular R3BP, for the corresponding value of μ.

In Fig. 3 we demonstrate more extensively the correlation between the choice of the initial conditions in the Floquet-Birkhoff normalized variables and the four possible transit properties (two transit and two non-transit family of orbits): the two families of initial conditions with $\mathcal{I}_3 > 0$ (red and green orbits) produce transit orbits, while the two family of initial conditions with $\mathcal{I}_3 < 0$ produce orbits which 'bounce' back when they approach the planar torus. This behavior is more clearly represented when we consider the projection of these orbits in the original xy variables. Again, the choice of the initial conditions have been done in the Floquet-Birkhoff normalized variables, and the numerical integrations have been done in the Cartesian variable as explained above for Fig. 1 and Fig. 2 (see caption of Fig. 3 for the initial conditions).

Figure 4 also show the effects caused of the variation of the anomaly f in the projection of the orbits to the Cartesian space. We appreciate that the effect of the eccentricity, through the variation of the anomaly in the terms of the transformation, is to generate a small time-dependent pulsation. Bottom left panel show with more detail such a pulsation on the $\mathcal{M}_{\mathcal{I}_1,0}$. A similar effect takes place when we consider the projection of the transit orbits. In these plots, we include also a family of orbits in the stable and unstable manifolds of $\mathcal{M}_{\mathcal{I}_1,0}$ (gray orbits). The initial conditions for the orbits in these manifold tubes have been chosen in the Floquet-Birkhoff normalized variables, by setting

$$\bigcup_{f,\phi\in[0,2\pi]} \{\Psi(\mathbf{Q},\mathbf{P},f;e) : (Q_1,P_1) = \sqrt{2\,\mathcal{I}_1}(\sin\phi,\cos\phi)\ ,\ P_3 \neq 0\ ,\ Q_2,P_2,Q_3 = 0\} \quad (61)$$

for the stable manifold tube, and

$$\bigcup_{f,\phi\in[0,2\pi]} \{\Psi(\mathbf{Q},\mathbf{P},f;e) : (Q_1,P_1) = \sqrt{2\,\mathcal{I}_1}(\sin\phi,\cos\phi)\ ,\ Q_3 \neq 0\ ,\ Q_2,P_2,P_3 = 0\} \quad (62)$$

for the unstable manifold tube.

In Fig. 8 we finally provide an example of transit orbits in the genuine spatial problem. The choice of the initial conditions is done exactly as for the planar transit orbits (60), except that we set $\mathcal{I}_1 = 0$ and $\mathcal{I}_2 > 0$, $\mathcal{I}_3 > 0$. The value of κ is the largest value considered for the orbits of Fig. 7, i.e. $\kappa(I_P) = 4.53968 \times 10^{-4}$.

5   Conclusions

The transits through the Lagrangian points of the circular restricted three-body problem are relevant for the dynamics of comets and spacecrafts. To use the results obtained for
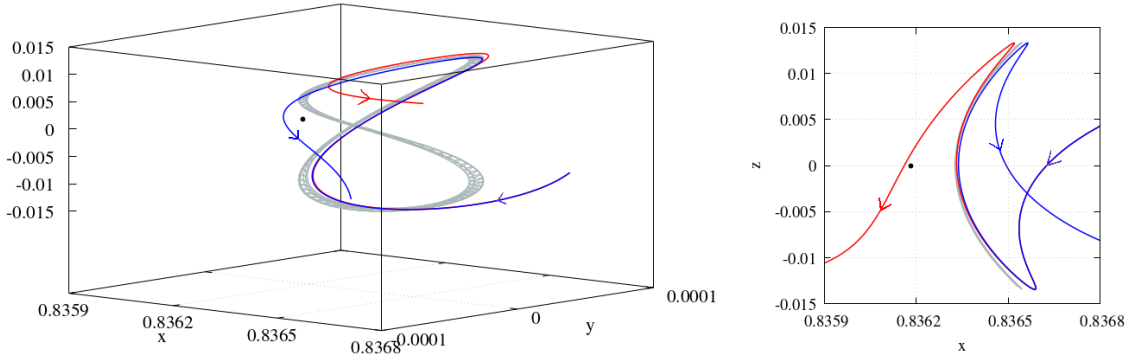
Figure 8: Two orbits of the spatial problem with very close initial conditions, but different transit properties. In the left-panel we represent the orbits in the Cartesian 3-dimensional xyz space, while in the right-panel we represent the projection of the orbits in the Cartesian 2-dimensional xz plane. The initial conditions are: $Q_1, P_1 = 0$, $Q_2 = 0$, $P_2 = 1/50$, and $f = 0$ for the two orbits, while $Q_3 = -1\times10^{-6}$, $P_3 = 1\times10^{-4}$ for the blue orbit and $Q_3 = 1\times10^{-6}$, $P_3 = 1\times10^{-4}$ for the red orbit. The gray orbit corresponds at the section $f = 0$ of the torus $\mathcal{M}_{0,\mathcal{I}_2}$. The arrows indicate the direction of the motion for increasing values of f.

the CRTBP in a realistic model of the Solar System requires to take into account the elliptic orbit of the planet of the close encounter, as well as the perturbations from the other planets. Despite the eccentricity of the planets is small, the ERTBP represents a major modification of the CRTBP, since non global first integral are known, and the definition of realms of admissible or forbidden motion and of the zero velocity curves is lost. Nevertheless the Lagrange solutions exist for both problems, and using a combination of the Floquet theory and of Birkhoff normalizations we have been able to recover a classification of the transits occurring at the Lagrangian points L_1, L_2. We have shown that an improvement of the traditional Floquet theory is indeed possible, except for few values of the reduced mass μ corresponding to resonances. These methods allow a full control of the effect to the true anomaly f (to use as a parameter) in the classification of the transits, and provide an analytic way to construct, for example, patched orbits more reliable than those of the bi-circular models. This is left for future works, as well as an analysis of the Arnold diffusion due to the remainder of Birkhoff normal forms, along the lines of paper [19].

Acknowledgments

References

[1] Amato D., Baù G., Bombardelli C., Accurate orbit propagation in the presence of planetary close encounters, *MNRAS* **470**(2), p 2079 (2017)

[2] Barrabés E., Gómez G., Mondelo J.M., Ollé M., Pseudo-heteroclinic connections between bicircular restricted four-body problems, *MNRAS* **462**(1), p 740750 (2016).

[3] Benettin G., Galgani L., Giorgilli A., Strelcyn J.-M., Tous les nombres caracteristiques de Lyapunov sont effectivement calculables, *Comptes Rendus Acad. Sc. Paris* **286A**, p 431 (1978).

[4] Capiński M.J., Gidea M., de la Llave R., Arnold diffusion in the planar elliptic restricted three-body problem: mechanics and numerical verification, *Nonlinearity* **30**(1), p 329 (2016).

[5] Cardin F., Guzzo M., Integrability of the spatial three-body problem near collisions (an announcement), *Rend. Lincei, Mat. Appl.* **30**, p 195 (2019).

[6] Cardin F., Guzzo M., Integrability of the spatial three-body problem near collisions, *arXiv:1809-01257* (2018).

[7] Ceccaroni M., Celletti A. Pucacco G., Halo orbits around the collinear points of the restricted three-body problem. *Physica D* **317**, p 28 (2016).

[8] Celletti A., Pucacco G., Stella, D., Lissajous and Halo orbits in the Restricted Three-Body Problem, *J. Nonlinear Science* **25**(2), p 343 (2015).

[9] Conley C., Low Energy Transit Orbits in the Restricted Three-Body Problems, *SIAM J. Appl. Math.* **16**(4), p 732 (1967).

[10] Efthymiopoulos C., Canonical perturbation theory, stability and diffusion in Hamiltonian systems: applications in dynamical astronomy, in *3rd La Plata International School on Astronomy and Geophysics "Chaos, Diffusion and Non-integrability in Hamiltonian Systems - Aplications to Astronomy"* (1st edition), Cincotta, P., Giordano, C., Efthymiopoulos, C., *eds.*, Uni. Nac. de la Plata, La Plata (2011).

[11] Floquet G., Sur les équations différentielles linéaires à coefficients périodiques *Ann. Ecole Normale Sup. Ser 2* **12**, p 47 (1883).

[12] Font J., Nunes A., Simó C., Consecutive quasi-collisions in the planar circular RTBP, *Nonlinearity* **15**, p 115 (2002).

[13] Giorgilli A., On a theorem of lyapounov, *Rendiconti dell?Instituto Lombardo Academia di Scienze e Lettere* **146**, p 133 (2012).

[14] Giorgilli A., Notes on exponential stability of Hamiltonian systems, in Dynamical Systems. Part I: Hamiltonian Systems and Celestial Mechanics (1st edition), *Pubblicazioni della Classe di Scienze, Scuola Normale Superiore, Centro di Ricerca Matematica "Ennio De Giorgi"*, Pisa (2003).

[15] Gómez G., Jorba À., Masdemont J., Simó C., Dynamics and Mission Design Near Libration Point Orbits, Vol. 3: Advanced Methods for Collinear Points, *World Scientific*, Singapore (2000).

[16] Gómez G., Koon W.S., Lo M.W., Marsden J.E., Masdemont J., Ross S.D., Connecting orbits and invariant manifolds in the spatial restricted three-body problem, *Nonlinearity* **17**, p 1571 (2004).

[17] Guardia M., Kaloshin V., Zhang J., Asymptotic Density of Collision Orbits in the Restricted Circular Planar 3 Body Problem, *Archive for Rational Mechanics and Analysis* **233**(2), p 799 (2019).

[18] Gronchi G., Tardioli C., The evolution of the orbit distance in the double averaged restricted 3-body problem with crossing singularities, *Disc. Cont. Dyn. Syst. B* **18**(5), p 1323 (2013).

[19] Guzzo M., Efthymiopoulos C., Páez R.I., Semi-analytic computations of the speed of Arnold diffusion along single resonances in a priori stable Hamiltonian systems, *J. Nonlin. Science* **30**, p 851 (2020).

[20] Guzzo M., Lega E., On the identification of multiple close-encounters in the planar circular restricted three body problem, *MNRAS* **428**, p 2688 (2013).

[21] Guzzo M., Lega E., A study of the past dynamics of comet 67P/Churyumov-Gerasimenko with fast Lyapunov indicators, *Astron. Astrophys.* **579**, A79 (2015).

[22] Guzzo M., Lega E., Scenarios for the dynamics of comet 67P/Churyumov-Gerasimenko over the past 500 kyr, *MNRAS* **469**, p S321 (2017).

[23] Guzzo M., Lega E., Geometric chaos indicators and computations of the spherical hypertube manifolds of the spatial circular restricted three-body problem, *Physica D* **373**, p 38 (2018).

[24] Jorba A., Begoña N., Transport and invariant manifolds near L_3 in the Earth-Moon bicircular model, *Commun. Nonlin. Science Num. Sim.* **89**, p 105327 (2020).

[25] Jorba A., Jorba-Cuscó M., Rosales J.J., The vicinity of the Earth-Moon L_1 point in the bicircular problem, *Celest. Mech. Dyn. Astron.* **132**, p 11 (2020).

[26] Jorba A., Masdemont J., Dynamics in the center manifold of the restricted three-body problem, *Physica D* **132**, p 189 (1999).

[27] Koon W.S., Lo M.W., Marsden J.E., Ross S.D., Dynamical Systems, the three body problem and space mission design. *Marsden Books*. ISBN 978-0-615-24095-4 (2008).

[28] Lega E., Guzzo M., Froeschlé C., Detection of close encounters and resonances in three-body problems through Levi-Civita regularization, *MNRAS* **418**, p 107 (2011).

[29] Lega E., Guzzo M., Three-dimensional representations of the tube manifolds of the planar restricted three-body problem, *Physica D* **325**, p 41 (2016).

[30] Le Verrier U.J., Théorie de la comete périodique de 1770, *Annales de l'Observatoire imperial de Paris, Memoires, t. 3. Paris: Mallet-Bachelier*, p. 203, 1-12, (1857).

[31] Markeev A.P., Libration points in celestial mechanics and astrodynamics, *Izdatel'stvo Nauka*, Moscow, (1978).

[32] Markeev A.P., A constructive algorithm for the normalization of a periodic Hamiltonian, *J. Appl. Math. Mech.* **69**, p 323 (2005).

[33] Masdemont J.J., High Order Expansions of Invariant Manifolds of Libration Point Orbits with Applications to Mission Design, *Dyn. Syst.*, **20**(1), p 59 (2005).

[34] Meyer K., Hall G., Offin D., Introduction to Hamiltonian Dynamical Systems and the N-Body Problem, *Springer-Verlag*, New York (2009).

[35] Oshima K., Topputo F., Yanao T., Low-energy transfers to the Moon with long transfer time, *Celest. Mech. Dyn. Astron* **131**, art 4 (2019).

[36] Palacián, J.F., Yanguas, P.: Invariant manifolds of spatial restricted three-body problems: the lunar case, in *Delgado, J. Lacomba, E.A., Llibre J., Pérez Chavela E. (eds.) New Advances in Celestial Mechanics and Hamiltonian Systems*, p 199. Kluwer Academic/Plenum Publishers, Dordrecht (2004).

[37] Páez R.I., Guzzo M., A study of temporary captures and collisions in the Circular Restricted Three-Body Problem with normalizations of the Levi-Civita Hamiltonian, *I. J. Nonl. Mech.* **120**, p 103417 (2020).

[38] Pucacco G., Structure of the centre manifold of the L_1, L_2 collinear libration points in the restricted three-body problem, *Cel. Mech. and Dyn. Astr.* **131**, art. 44 (2019).

[39] Sanders J., Verhulst F., Murdock J., Averaging Methods in NonLinear Dynamical Systems, *Springer-Verlag*, New York (2007).

[40] Scantamburlo E., Guzzo M., Short-period effects of the planetary perturbations on the Sun-Earth Lagrangian point L_3, *Astron. Astrophys.* **638**, A137 (2020).

[41] Simó C., Dynamical systems methods for space missions on a vicinity of collinear libration points, in *Simó, C., editor, Hamiltonian Systems with Three or More Degrees of Freedom (S'Agaró, 1995), volume 533 of NATO Adv. Sci. Inst. Ser. C Math. Phys. Sci.*, p 223, Dordrecht. Kluwer Acad. Publ. (1999).

[42] Valsecchi G.B., Close Encounters in Öpik Theory, in *Lecture Notes in Physics, Singularities in Gravitational Systens, D. Benest and Cl. Froeschlé editors*, Springer (2002).

[43] Valsecchi G.B., Close encounters and collisions of Near-Earth asteroids with the Earth, *C. R. Physique* **6** (2005).

[44] Vanzelli D., Stabilità alla Nekhoroshev di orbite periodiche transversalmente ellittiche con applicazione al problema dei tre corpi ristretto ellittico, *Master thesis*, Università degli Studi di Padova (2011).

[45] Wiesel, W.E., Pohlen D.J., Canonical Floquet Theory, *Celest. Mech. and Dyn. Astron.* **58**, p 81 (1994).

[46] Zanzottera A., Castelli R., Mingotti G., Dellnitz M., Intersecting invariant manifolds in spatial restricted three-body problems: Design and optimization of Earth-to-halo transfers in the Sun-Earth-Moon scenario, *Commun. Nonlin. Science Num. Sim.* **17**(2), p 832 (2012).